Theses and Dissertations

2024-11-07

Biodegradable Polymeric Microspheres for Magnetically Guided Drug Delivery to Tumors

Tyler Payson Green
Brigham Young University

Follow this and additional works at: https://scholarsarchive.byu.edu/etd

Part of the Engineering Commons

Biodegradable Polymeric Microspheres for Magnetically

Guided Drug Delivery to Tumors

Tyler Green

A thesis submitted to the faculty of
Brigham Young University
in partial fulfillment of the requirements for the degree of

Master of Science

William G. Pitt, Chair
Bradley C. Bundy
Thomas A. Knotts

Department of Chemical Engineering

Brigham Young University

Abstract

This thesis investigates the feasibility of utilizing biodegradable polymeric microspheres loaded with the anticancer drug 5-fluorouracil (5FU) and superparamagnetic iron oxide nanoparticles (SPIONs) to magnetically deliver the cancer therapeutic 5FU to a target tumor in the human body. The primary method of material loading consisted of a w/o/w double emulsion mechanism which 1) loads and protects 5FU in the inner water phase consisting of distilled water and polyvinyl alcohol (PVA), 2) dispersed SPIONs in the biodegradable polymeric organic phase consisting of methylene chloride ($MeCl_2$) for eventual magnetic transport, and 3) suspended these w/o emulsion droplets in an outer aqueous phase comprised of water and PVA and then evaporating the solvent by convection.

This procedure produced dried double emulsion microspheres below 2 μm in diameter. They were characterized using scanning electron microscopy (SEM), and magnetometry, which demonstrated their size and superparamagnetic properties. The encapsulation efficiency of 5FU into these polymeric microspheres was above 95%. Drug release of 5FU from dried double emulsion microspheres was significant over 63 days in water and phosphate buffered saline (PBS). Drug release was faster at 37 °C compared to room temperature (21 °C). The medium of PBS at pH 7.4 and 5.4 promoted faster release than distilled water at pH 7.0. Release was faster from PLGA than from PLA. Antibiotic potency of 5FU remained effective after drug release and degradation of carrier. Application of these microspheres in future clinical trials may present a noninvasive, low-risk method to treating malign tumors in nonresectable regions while demonstrating more effective results than systemic administration of chemotherapy. This research presents a significant innovation in therapeutic drug delivery technology for nonresectable cancerous tumors, particularly in the head and neck regions.

Keywords: drug delivery, controlled release, SPION, cancer therapy, head and neck cancer, magnetic transport

Acknowledgments

Table of Contents

List of Figures

List of Acronyms

5FU – 5-fluorouracil
DPD – dihydropyrimidine dehydrogenase
dTMP – deoxythymidine monophosphate
FDA – food and drug administration
FdUMP – fluorodeoxyuridine monophosphate
HNSCC – head and neck squamous cell carcinoma
HPMC – hydroxypropyl methyl cellulose
PLA – poly(lactic acid)
PLGA – poly(lactic-co-glycolic acid)
PVA – poly(vinyl alcohol)
SDS – sodium docecylsulfate
SEM – scanning electron microscopy
SPION – superparamagnetic iron oxide nanoparticle
TS – thymidine synthase

1   *Introduction*

The effort to treat cancerous tumors has promoted the development of numerous cancer therapy methods [1]. One of the most effective methods is surgical resection, which aims to completely extract a tumor from the patient [2]. However, current methods of tumor treatment like surgical resection are not always practical. The potential for morbidity or mortality of the patient prompted the genesis of a wide range of research with specific aims to overcome such barriers and explore alternatives or supplements to surgery [3, 4].

Head and neck tumors are among the most difficult to treat by surgery or radiation due to the proximity and tight packing of critical blood vessels, nerves, and vital conduits for eating and breathing, which complicate surgical resection and precise radiation treatment of tumors only [5]. Head and neck tumors are the sixth most frequent type of cancer worldwide with over 870,000 new cases and 440,000 deaths in 2020 [6]. Alternative treatments to surgery and radiation include systemic administration of chemotherapy, which causes whole-body side effects, and systemic dosing with microscale drug carriers using tumor-tissue-targeting molecules, which are still under development [7-11]. An effective and noninvasive treatment method for cancerous tumors in the head and neck region remains elusive and in high demand.

My master's thesis project aimed to create double emulsion microspheres for the delivery of anti-cancer drug to malignant tumors in the head and neck region through targeted magnetic drug delivery. By loading the microspheres with superparamagnetic iron oxide nanoparticles (SPIONs), the microcarriers may be injected into the circulatory system and magnetically pushed to the capillaries of a targeted tumor. The remainder of this report details the use of SPIONs and 5-fluorouracil (5FU), the characteristics of the polymeric microspheres produced by double emulsion, and the methods to determine drug loading, controlled drug release and drug potency after release.

2   Literature Review

This literature review presents the key points of the project: the challenge of treating head and neck tumors, the need for targeted drug delivery, 5-fluorouracil (5FU) as an anticancer drug, superparamagnetic iron oxide nanoparticles (SPIONs), and polymeric double emulsion microspheres for controlled drug release.

2.1   Difficulty of Treating Head/Neck Tumors

Primary symptoms of head and neck tumors, commonly called head and neck squamous cell carcinomas (HNSCCs), often share symptoms with benign illnesses such as pain in the throat and swelling [12, 13]. These misleading symptoms, along with inefficient standard screening methods, often delay accurate diagnosis [14]. Once appropriately diagnosed, therapy consists of surgical resection (if found in an early stage) followed by both chemotherapy and radiotherapy. Surgical removal is often difficult and sometimes impractical because of the high density of nerves, blood vessels, and other structures essential to speaking, eating and breathing. Post-surgical treatments impose intense patient discomfort due to local radiation treatment or to whole-body side effects of chemotherapy, and sometimes remain ineffective due to resistance of tumors to treatment [15, 16].

2.2   Targeted Therapy

Many efforts to improve the effectiveness of head and neck cancer treatment involve targeted therapy, including gene therapy, monoclonal antibodies, antibody toxin conjugates, small-molecule inhibitors, antisense molecules, and tumor vaccines [17]. Current targeted therapy methods for head and neck tumors often use monoclonal antibodies or antimetabolites. Whereas advances in radiochemotherapy have increased 5-year survival rates of head and neck cancer patients from 6.5% in 2004 to 36% in 2019, therapy involving the use of monoclonal antibodies raises the 5-year survival rate to 45% as reported by Sindu et al. in 2019 [18, 19]. However, tumor-targeting therapy using monoclonal antibodies often aims only to inhibit tumor growth by targeting and interfering with the epidermal growth factor receptor (EGFR) which promotes tumor cell proliferation and metastasis [20-23]. Unlike therapy utilizing monoclonal antibodies, therapy using antimetabolites aims to achieve a similar effectiveness to surgical resection

by killing the cancer cells through cytotoxic interference with tumor functions rather than just inhibiting their growth [24]. This thesis examines the use of 5-fluorouracil, an antimetabolite, to maximize the results of a potentially more effective targeted therapy mechanism compared to current literature.

2.3   5-Fluorouracil as an Anti-cancer Drug

5-Fluorouracil (5FU) is a common antimetabolite cancer drug used currently for intravenous cancer chemotherapy and is the anti-cancer drug used in this project. 5FU kills tumor cells by being converted to fluorodeoxyuridine monophosphate (FdUMP), which inhibits deoxythymidine monophosphate (dTMP) by forming a stable complex with thymidine synthase (TS). Since dTMP is crucial for the replication and repair of DNA, its reduction or absence results in cytotoxicity and death in the tumor cells [25-28]. Studies analyzing the toxicity and biocompatibility of 5FU show that the liver primarily metabolizes 5FU into inactive degradation products while the remainder of the parent drug is excreted in the urine within 6 hours after intake with a mean biological half-life of about 16 minutes. However, 5FU is a considerably potent antimetabolite which necessitates restrictions regarding the patients to whom the drug will be administered, reducing the pool of clinical application. The same studies report the potential and truly severe toxic reactions to 5FU that occur in pregnant patients and patients with dihydropyrimidine dehydrogenase enzyme (DPD) deficiency, which is an enzyme mutation that occurs in 3-5% of the overall population. This potential risk therefore promotes clinical confirmation of no DPD deficiency in the patient before administration of 5FU [29-32]. Despite these restrictions, 5FU is a prominent antimetabolite that is on the list of key drugs that are essential for treating breast, stomach, skin, colorectal, and esophageal cancer. Therefore, it was selected for use in this project.

2.4   Superparamagnetic Iron Oxide Nanoparticles in Literature

There is much interest in using super paramagnetic nanoparticles for therapeutic intervention. Superparamagnetic nanoparticles are characterized by two requirements. First, the particles exhibit a strong magnetic moment while in the presence of an external magnetic field so they can be spatially manipulated. Second, its magnetization curve shows no hysteresis, meaning that when removed from an external magnetic field the sample exhibits zero magnetization. This characteristic prevents superparamagnetic materials from agglomerating to each other except in the presence of an external magnetic field. Superparamagnetic properties have been observed in magnetite iron oxide (Fe_3O_4) nanoparticles, prompting the development of many biomedical applications including magnetically guided therapies [33-35].

2.4.1 Superparamagnetic Iron Oxide Nanoparticles in Magnetic Drug Delivery

A novel application of SPIONs is targeted magnetic drug delivery. By pairing an anti-cancer drug with SPIONs, the drug may be spatially manipulated by an external magnetic field. When injected into the vasculature, drug-loaded superparamagnetic microcarriers may be magnetically pushed with high-gradient permanent magnets to a target area of accumulation in a tumor [36, 37]. The head and neck regions are optimal for magnetically guided drug delivery because of facile placement of multiple external devices to create orthogonal magnetic fields for 3D focusing using a Halbach array. A Halbach array contains a particular orientation of permanent magnets in 2D and 3D orientations to apply forces directed to volumes other than attraction to the surface of a magnet. This can be used to push magnetic nanoparticles to deeper tissue locations than the skin [38]. This design has a maximum working depth of about 10 cm (which is within the working distance for head and neck tumors) and purports sufficient magnetic force to trap microcarriers containing SPIONs in the capillaries of a tumor, whereupon they can slowly release their therapeutic payload.

Such forces may push and perhaps lodge particles to the internal lumen side of a capillary when tangential magnetic forces exceed the low axial fluid drag force on sufficiently small particles. Al-Jamal et al. studied the effect of SPION loading on blood circulation in mice and extrapolated his findings to humans. They performed this study with reference to the finite element model presented by Nacev et al. using blood and blood vessel information from the Phase I clinical study of Lübbe et al. [39-41]. These studies concluded that external magnetic forces would be sufficient to achieve successful targeting in humans, further transitioning magnetic drug delivery research from its preclinical study stage to proposed clinical applications.

2.4.2 Biocompatibility of Superparamagnetic Iron Oxide Nanoparticles as Drug Carriers

Studies of SPIONs have analyzed their toxicity in the human body prior to the beginning phases of their approval by the FDA. These studies indicate low or no cytotoxicity of SPIONs for both *in-vivo* animals and human stem cell studies and reveal both a short-term and long-term biocompatibility with no apparent acute or chronic toxicity in mice *in-vivo* [42-44]. Iron oxide slowly dissolves, and the Fe^{3+} or Fe^{2+} is used by the body or excreted in urine if in excess.

2.5 Polymeric Double Emulsion Particles for Controlled Drug Release

Drug sequestration and controlled release are vital features of anti-cancer drug delivery systems. Many drug delivery systems employ polymeric carriers to simultaneously control the rate of degradation and to protect the

encapsulated drug from any adverse microenvironment of the body before reaching the target area [45]. For anti-cancer drug delivery, these polymeric structures are often comprised of the biodegradable polymers polylactic acid (PLA), polyglycolic acid (PGA), or poly(lactic-co-glycolic) acid (PLGA). The degradation of these polymers occurs by hydrolysis and polymer chain cleavage, eventually forming lactic acid and glycolic acid, which are made and consumed in normal body metabolism. PLGA is usually a less crystalline polymer structure than PLA, suggesting that PLA might degrade more slowly than PLGA. While release may be controlled through the shape (dimensions), composition, and molecular weight of polymer, loading and entrapment rely on a more complex system of meta-stable phase separation in multiple emulsions, and the stability of those phases during drying [46-48].

Small polymeric spherical drug carriers can be made via a double emulsion process, which combines a single emulsion with an additional phase to entrap many droplets of the first emulsion within individual droplets of the second emulsion, as illustrated in Figure 1 [46, 49, 50]. State-of-the-art literature reports nonmagnetic PLA microspheres produced by double emulsion containing anticancer drug under 2 μm in diameter and microspheres composed of a SPION core and a drug-loaded PLA shell under 10 nm in diameter [51, 52]. An advantage to this entrapment method is that each phase of the emulsion may contain a different key chemical or drug, also depicted in Figure 1. This advantage may ensure more effective protection and sequestration of an anti-cancer drug like 5-fluorouracil (5FU) during its transport through the body to a target location, while simultaneously achieving greater control over the degradation mechanism through multiple phases of polymer [48, 53].
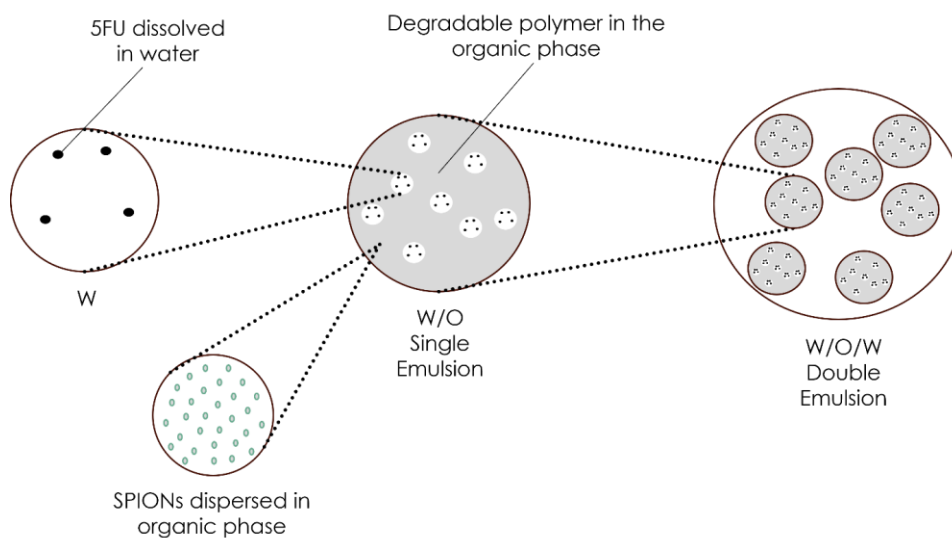
Figure 1: Illustration of a double emulsion. This production begins with a water phase (white) containing dissolved drug 5FU (black) which is then dispersed in a degradable polymer dissolved in a hydrophobic solvent (organic phase, gray) which also contains dispersed SPIONs to form a single w/o emulsion. This single

emulsion is then dispersed in a final phase of water (white) to form the double emulsion, following which the solvent and water are slowly removed by evaporation from the phases to form spherical particles.

The drug release rate of a carrier composed of PLA is controlled by the rate of polymeric degradation caused by ester hydrolysis in the polymer in the presence of water. Hydrolysis starts on the polymer surface and, as water diffuses into the polymer, deeper internal polymer chains are also cleaved. As degradation occurs, cancer drug trapped in the organic phase is exposed to and is released into the surrounding water medium. This degradation process subsequently increases the surface area of the degrading particle and sometimes increases degradation and drug release at an accelerating rate. The drug protection offered by these polymeric particles offers the benefit of reducing adverse side effects to the patient normally caused by early or rapid release, or the reaction of a therapeutic drug in unintended tissues of the body. These benefits render this method of drug delivery safer for patients in addition to using its advanced drug entrapment efficiency, delivery effectiveness, and overall controllability [54, 55]. Current research continues to improve the reliability and application of this method, ensuring a more uniform size distribution of microspheres collected from the double emulsion manufacturing process [47].

3   *Thesis Objectives*

The overall goal of this thesis research was to prepare double emulsion polymeric microspheres containing both SPIONs and 5FU under a threshold of 5 µm in size for effective magnetic drug delivery. This goal contained several objectives to ensure the effectiveness of the contents and of the degradation process, as well as to ensure accurate particle size and drug potency. The first three objectives below pertain to the composition and quality of the microspheres. The remaining objectives are related to the effectiveness of the microspheres as drug carriers. The objectives were as follows:

1. Synthesize superparamagnetic nanoparticles about 8 nm in diameter through thermal decomposition for loading into double emulsions.
2. Form w/o/w double emulsion polymeric microspheres comprised of PLA and poly(vinyl alcohol) (PVA) with a target size below 5 µm in diameter as carriers for 5FU and SPIONs.
3. Load polymeric microspheres with 5FU inside the inner aqueous phase and SPIONs inside the biodegradable polymer phase while maintaining overall particle size below the 5 µm diameter threshold.
4. Determine the encapsulation efficiency of 5FU into the polymeric microspheres
5. Determine drug release kinetics of 5FU from the polymeric microspheres.
6. Confirm antibiotic potency of 5FU after release from the polymeric microspheres.

4   *Superparamagnetic Iron Oxide Nanoparticles*

4.1   Superparamagnetic Iron Oxide Nanoparticle Synthesis

SPIONs were synthesized using the thermal decomposition method published by Sun et al. with a target size of around 8 nm-diameter [56]. Briefly, the particles were prepared by combining oleic acid, oleylamine, Tris(acetylacetonato)iron(III) (*Fe(acac)$_3$*) and 1,2-hexadecanediol with constant magnetic stirring and a flow of nitrogen. The mixture was heated to 200 °C for 2 hours and then heated to 300 °C and refluxed for 1 hour. The resulting particles were then rinsed 5 times with ethanol and placed in a vacuum desiccator to dry for 24 hours to form a dry powder.

4.2   Superparamagnetic Iron Oxide Nanoparticle Characterization

The SPIONs were characterized by transmission electron microscopy (TEM, Tecnai, TF-20, FEI, Hillsboro, OR, USA) with the assistance of personnel in the BYU physics department and also by vibrating sample magnetometry (VSM, Quantum Design, San Diego, CA, USA) on which field cooling and zero field cooling (FC/ZFC) measurements were carried out, as well as magnetization loops that reveal possible magnetic hysteresis. Magnetometry was done with the assistance of Rajendra Gautam of the BYU physics department.

Synthesized SPIONs were imaged with TEM (Figure 2a) and found to have a size distribution of 8.8 ± 1.9 nm evaluated over at least 100 particles. As seen in the TEM image 2a, this batch of SPIONs is polydisperse, and includes some large particles (the maximum size observed in the TEM images is 18 nm) mixed with the smaller particles.

The magnetometry characterization shown in Figure 2b,c suggests that the SPIONs are superparamagnetic (SPM) at 300 K. The field cooling (FC) and zero field cooling (ZFC) curves in Figure 2b indicate a blocking temperature spread around $T_B \sim 185$ K (spreading from about 90 K through 300 K at 90 % of max ZFC value). The wide spread and relatively high median value for T_B is likely due to the wide spread in particle sizes and the heavier weight taken by the bigger particles, as the magnetic moment measured here via VSM is proportional to the volume (not the diameter) of the particles. When the average is based on particle volume (3rd moment of particle size distribution), the average nanoparticle size is 9.3 ± 2.7 nm. The bigger particles induce strong magnetic interparticle interactions with the

surrounding particles, and these interactions are weighted more heavily in the case of these SPIONs that are placed in the VSM capsule.
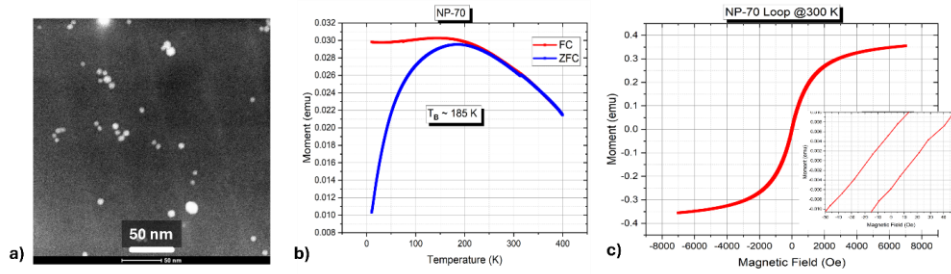
Figure 2: Structural and VSM magnetic characterization of SPIONs. (a) TEM image of the fabricated SPIONs sparsely dispersed on a TEM grid. (b) FC-ZFC curves collected under a magnetic field of 100 Oe. (c) Magnetization loop collected at 300 K over ± 7000 Oe range, with a zoomed-in view around the origin in the inset.

Lastly, the magnetization loop collected at 300 K in Figure 2c shows no substantial hysteresis when plotted over a range of ± 7000 Oe. When zoomed-in over a ± 50 Oe range, a very small hysteresis, smaller than 20 Oe appears, but given the uncertainty of measurement, this hysteresis is considered negligeable and confirms superparamagnetism at 300 K measured by ZFC curves (Fig 2b).

Figure 3 shows magnetometry data for the SPIONs after being embedded in the microspheres. The FC-ZFC curves in Figure 3a now suggests a much lower blocking temperature ($T_B \sim 75$ K), which typically corresponds to what has been observed for isolated, non-interacting, monodisperse nanoparticles with an average size around 8 nm [57, 58]. In addition, the value of the measured magnetic moment (on the y-axis) is now about a factor of 100 smaller than what it was for the naked SPIONs in Figure 2b. These observations suggest that the SPIONs are well diluted (not aggregated) within the PLA microspheres, thus practically eliminating magnetic interparticle interactions. The magnetization loop collected at 300 K in Figure 3b shows no substantial hysteresis when plotted over a field range of ± 7000 Oe. The zoomed in view over a ± 50 Oe in Figure 3c shows a very small hysteresis (less than 30 Oe), which given experimental uncertainty is sufficiently small to assume the material is nearly superparamagnetic at 300 K. In summary, the present SPIONs show nearly superparamagnetic behavior at 300 K both in their naked form and once embedded in the microspheres. They appear to be embedded as discrete particles, as opposed to aggregates of particles.
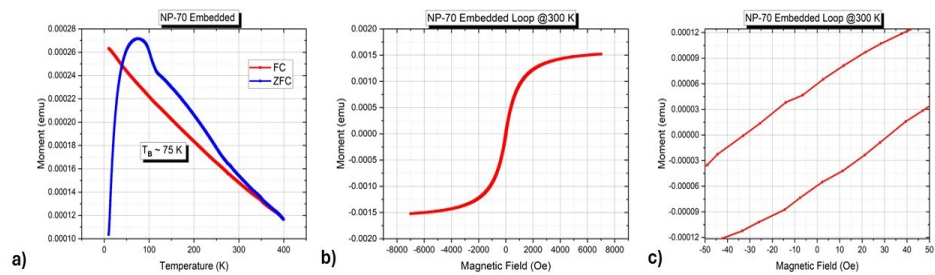
Figure 3: VSM magnetic characterization of SPIONs embedded in microspheres. (a) FC-ZFC curves collected under a magnetic field of 100 Oe. (b) Magnetization loop collected at 300 K over ± 7000 Oe range (c) Zoomed-in view around the origin, over ± 50 Oe range.

5 *PLA Microspheres by Double Emulsion Process*

5.1 Double Emulsion Synthesis

The standard process to form double emulsion microspheres proceeded as follows. The first (inner) water phase was formed by dissolving 5FU at saturation concentration (12 mg/mL) into a solution of PVA in distilled water. The organic phase was prepared by dissolving 3.0 g of PLA (or PLGA) in 17 mL of $MeCl_2$. A suspension of SPIONs in $MeCl_2$ was made by dispersing 10 mg of SPIONs (9 nm in diameter) in 20 mL of $MeCl_2$ by sonication for 1 hour in a sonicating bath (Sonicor, SC-100, Wallingford, CT, USA). Then 1.0 g of this SPION dispersion was added to 4.0 g of the PLA/$MeCl_2$, resulting in 0.088 mg of SPIONs per mg of organic phase and 0.094 mg of PLA per mg of organic phase. This mixture was vortexed for one minute.

A second (outer) aqueous phase was prepared, consisting of a surfactant dissolved in distilled water.

The w/o emulsion was formed by adding 0.125 g of the 5FU solution (first inner aqueous phase) to 4.875 g of the organic phase and emulsifying the phases for one minute to form submicron droplets by one of the various techniques described below. Then 1.0 g of this w/o microemulsion was added to 4.0 g of the second (outer) aqueous solution followed by similar emulsification. This w/o/w emulsion was dried by natural convection evaporation at room temperature in a fume hood for 24 hours to slowly remove the $MeCl_2$. The mass lost during this drying process was recorded. Distilled water was added to replace the mass lost during this quiescent drying. The emulsion was then redispersed by the same method of sonication and slowly dried by natural convection at room temperature in a fume hood for 48 hours.

5.2 Experimental Design

Double emulsion (w/o/w) microspheres were synthesized with the target size of less than 5 μm in diameter. Various experiments were performed to obtain the parameters necessary to evolve the procedure framework in Section 5.1 to the final optimal procedure described in Section 5.4. These experiments optimized the parameters of the procedure to achieve a consistent and uniform particle size below 5 μm in diameter.

5.2.1 Emulsion Ratios

The mass ratios of the above formulation (Section 5.1) are 0.5:19.5:80.0 (inside-aqueous-phase:organic-phase:outside-aqueous-phase). The effects of changing these phase ratios in the above procedure were examined by varying the mass ratio of the inner water phase to the organic phase in the first w/o emulsion and by varying the mass ratio of the first w/o emulsion to the outer water phase in the w/o/w emulsion.

5.2.2 Emulsification Methods

The method of emulsifying the substances for both the w/o and the w/o/w emulsions comprised three techniques: a magnetic stir bar, sonicating probe (Sonics and Materials Inc., Model CV26, Newtown, CT, USA), or mechanical emulsifier (Ultra Turrax, T25 Basic with Model S25N-8G probe, IKA, Wilmington, NC, USA).

5.2.3 Surfactant Chemical

The surfactant species in the water phases were varied to determine which produced optimal results. Candidate surfactants were PVA, sodium dodecyl sulfate (SDS), and Brij O20 in the inner and outer water phases of the double emulsion. PVA was examined because it was used as a surfactant in the procedure published by Delie et al. which encapsulates material within PLA microparticles [50]. SDS was examined due to its hydrophilicity and long hydrocarbon chain which could inhibit liquid droplets from merging with one another. Brij was examined because it is a polyethylene glycol-based surfactant like that used in the procedure published by Debotton et al. encapsulating drug in double emulsions [48].

5.2.4 Surfactant Concentration

The concentrations of surfactant in the inner and outer water phases of the double emulsion were also varied, as was the concentration of 5FU in the inner water phase.

5.2.5 Drying Methods

Experiments were performed to determine the optimal drying method for the double emulsion, including convection drying in a fume hood, convection drying in a fume hood with a stir bar inside the vessel, and freeze drying (LABCONCO FreeZone 2.5). The drying vessel was also examined, including 20 mL scintillation vials, petri dishes, and watch glasses.

5.3 Double Emulsion Characteristics

Various trials were performed by varying the parameters and equipment as outlined in the experimental design to minimize diameter size and optimize uniformity of product microspheres synthesized by the double emulsion method. Double emulsion particles were dried and then examined by scanning electron microscopy (SEM, Apreo, C Low-Vacuum,

ThermoScientific, Waltham, MA, USA). ImageJ (NIH, Bethesda, MD, USA) was used to determine the diameter size of the product double emulsion particles observed by SEM imaging. From this data, the maximum and minimum diameters, average diameter, and the polydispersity index were calculated for several analyzed samples. The polydispersity index was calculated as the standard deviation of the particle population diameter divided by the mean average diameter of the particle population.

5.3.1 Emulsion Ratios

Various experiments were performed to determine the emulsion ratios for the single and double emulsions which would minimize the size of the emulsion microspheres. For the first w/o emulsion, the ratios of 10:90, 5:95, and 2.5:97.5 w:o were examined and are shown in Figure 4. The droplets observable by light microscopy decreased in diameter as the fraction of the first (inner) aqueous phase decreases in the w/o emulsion. Of the ratios tested, the w/o emulsion ratio which best minimizes the diameter of the droplets is 2.5:97.5 w:o.
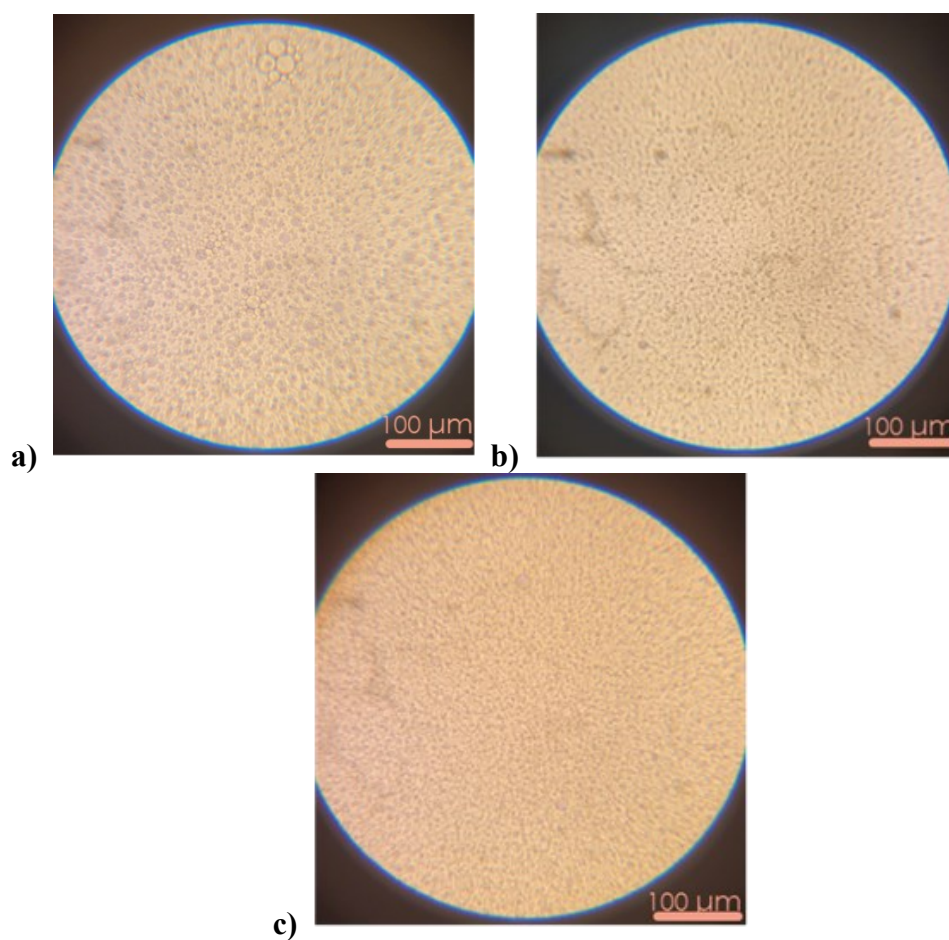
Figure 4: Visible light microscopy images of w/o emulsions with 9 wt% PVA in the inner water phase and mixed by sonicating probe depicting the relative size of droplets in an emulsion ratio of **a)** 10:90 w:o, **b)** 5:95 w:o, **c)** 2.5:97.5 w:o.

The average droplet diameter size decreases with a decrease in the fraction of the inner water phase in the w/o emulsion. While the goal of the project was to minimize the size of the double emulsion microspheres, the drug loading of the microspheres remained crucial. Therefore, a ratio needed to be selected which minimized the droplets to a sufficient degree and loaded the spheres with a significant mass of 5FU. The w/o emulsion ratio selected to meet these requirements was 2.5:97.5 w:o and was used for the remainder of this project. This ratio would load the emulsion with 0.03 wt% 5FU or 0.3 mg 5FU per mL of w/o emulsion, which is a significant concentration of 5FU when compared to the mass of 5FU reported to deliver to hepatocellular tumors in the body by typical clinical dosage of systemic administration in current research at 0.79 µg/day [59, 60].

As the double emulsion consists of droplets of w/o emulsion dispersed within a water medium, smaller w/o droplets will result in smaller w/o/w product microspheres. Figure 5 shows that the w/o/w droplet size decreases as the fraction of w/o decreases in the w/o/w double emulsion.
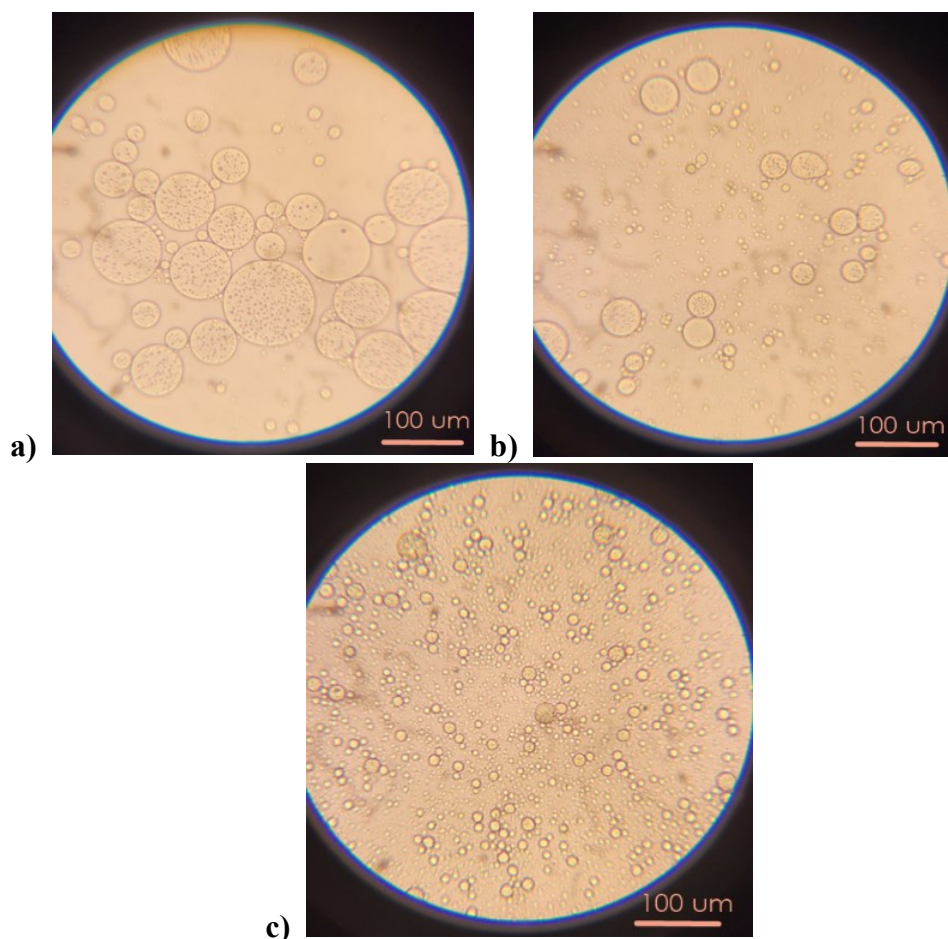
Figure 5: Visible light microscopy images of non-evaporated w/o/w emulsions with 1 wt% PVA in the outer water phase depicting the relative size of droplets in

an emulsion ratio of **a)** 50:50 w/o:w, **b)** 40:60 w/o:w, **c)** 20:80 w/o:w. Scale bars are 100 μm.

Figure 5 also shows that the w/o/w double emulsion ratio that minimizes the diameter of the droplets is 20:80 w/o:w. Further decreasing the fraction of w/o in the double emulsion will likely continue to decrease the size of the final product particles; however, the 20:80 ratio was satisfactory to reach an average diameter below 5 μm in the final product.

5.3.2   Emulsification Methods

Emulsification methods were compared to determine the method which best minimizes the final particle size. Emulsification by magnetic stir bar, emulsifier, and sonicating probe are compared in Figure 6.

a)   b)

c)
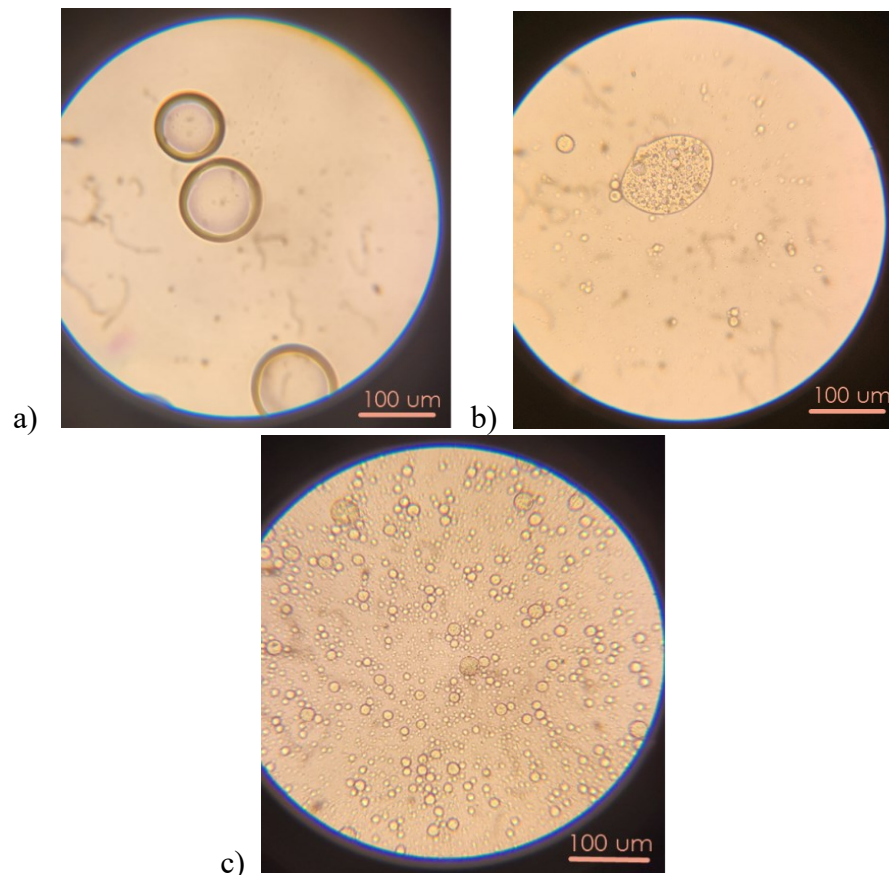
Figure 6: Visible light microscopy images of w/o/w emulsions with 1 wt% PVA in the outer water phase comparing the droplet size between samples emulsified with **a)** a magnetic stir bar, **b)** an emulsifier (Ultra Turrax T25 Basic with Model S25N-8G probe), **c)** a sonicating probe (Sonics and Materials Inc. Model CV26).

According to Figure 6a, experiments using a stir bar to emulsify the phases proved inadequate, producing w/o and w/o/w droplets observably macroscopic and too large for the purpose of this project. Additionally, the magnetic field of the stir bar caused the superparamagnetic double emulsion

droplets to accumulate onto the stir bar, preventing uniform emulsification. Experiments conducted using the Ultra Turrax emulsifier produced macroscopic w/o/w droplets much too large for this project as seen in Figure 6b. These macroscopic droplets were observed less frequently when prepared by emulsifier than when prepared by stir bar; however, the size distribution of droplets produced by the emulsifier were unsatisfactory for this project. Experiments which utilized the sonicating probe at an amplitude of 15% power (1.5 W/cm^2) to emulsify the phases produced microscopic w/o and w/o/w droplets. Figure 6c shows an average w/o/w droplet diameter of about 15 μm. Because the product diameter size is significantly smaller and more uniform when the double emulsion is emulsified using the sonicating probe, all subsequent experiments in this study were conducted using the sonicating probe to emulsify the phases.

5.3.3   Surfactant Chemical

Surfactants PVA, SDS, and Brij O20 were used to determine which best minimizes the average diameter and maximizes the morphological uniformity of the product microspheres. Figure 7 provides a comparison of the final double emulsion product using each of these substances.
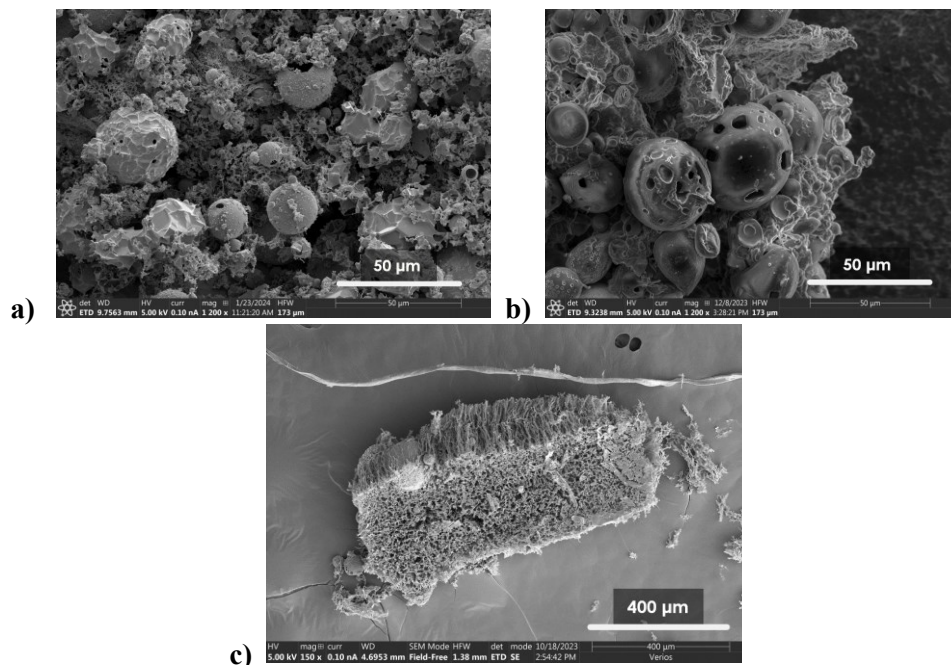
Figure 7: SEM images of double emulsion product particles with one surfactant in both water phases (9 wt% surfactant in inner water phase and 1 wt% surfactant in outer water phase) and prepared by freeze drying with various surfactants **a)** PVA, **b)** Brij O20, **c)** SDS.

The particles depicted in Figure 7 were produced by freeze drying the emulsified w/o/w suspension. This figure shows that double emulsions prepared with PVA as surfactant produced spherical particles with an

average diameter smaller than that of the other surfactants with some nonspherical, rigid product present. This rigid product was present only when the double emulsion with PVA surfactant was freeze dried, as discussed later in this study. Double emulsions prepared with Brij O20 as surfactant produced mostly nonspherical, agglomerated products unsatisfactory for this project. Emulsions prepared with SDS as surfactant produced large spherical particles entrapped by honeycomb-like matrices of SDS debris. Furthermore, SDS produced the largest product particles with the larger particles nearing 100 µm in diameter. Considering these results, the use of PVA as the surfactant produced the smallest and most uniformly spherical product up to 30 µm in diameter, the use of SDS produced microspheres up to 200 µm in diameter and surrounded by debris, and the use of Brij O20 produced nonspherical products. Therefore, PVA surfactant was observed to produce the morphology closest to that desired for this project and was selected for further studies.

Experiments utilizing Brij O20 as the surfactant occasionally produced double emulsion microspheres with overly porous surfaces as shown in Figure 8.
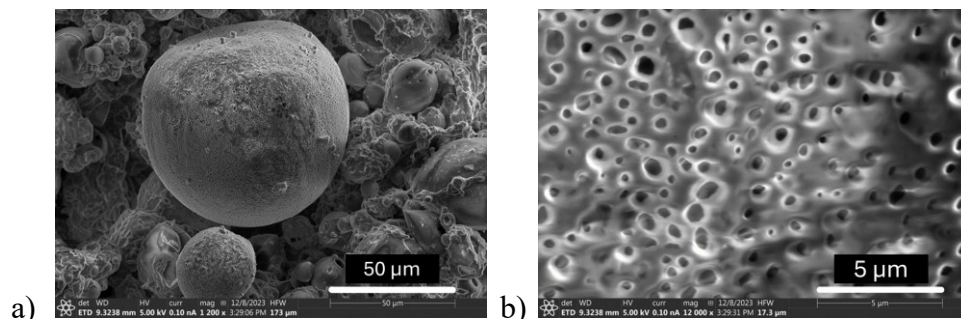
Figure 8: SEM images of double emulsion product particles with Brij O20 in both water phases (9 wt% in inner water phase and 1 wt% in outer water phase) prepared by freeze drying. a) 1,200x image of a large (~75 µm) microsphere. b) 12,000x close-up image of the surface of a large microsphere.

Figure 8a is a low-magnification image of a large, overly porous product particle and Figure 8b is a high-magnification image of the same particle. The pores in the double emulsion structure are formed by evaporation of the inner water phase of the emulsion. A higher quantity of pores in the structure provides more volume through which the medium may diffuse and cleave the polymeric microsphere, thereby increasing the degradation rate and subsequent drug release rate. Additionally, the presence of pores less than one micron in diameter with a narrow size distribution confirms that the w/o emulsion is sufficiently emulsified, with droplets of the inner water phase comparable in diameter size to the droplets observed in Figure 4c and the internal droplets within the larger structures observed in Figure 5c and Figure 6c. The porosity of the double emulsion microspheres may therefore be a significant parameter to optimize for very fast controlled drug release, but it is outside the scope of this project.

5.3.4 Surfactant Concentration

Macroscopic observations indicated that PVA concentration in the inner water phase was inversely related to the droplet diameter size. Thus, the saturation concentration of the PVA in water, 9 wt%, was used for the inner water phase for all subsequent experiments in this study. Trials were performed at different concentrations of PVA in the outer water phase to determine the effect of the surfactant on the product particle size, as shown in Figure 9. Associated SEM images of the product double emulsion microspheres are also included in Figure 9.
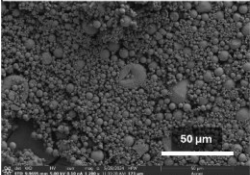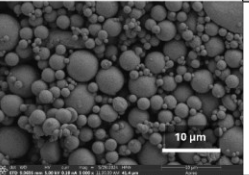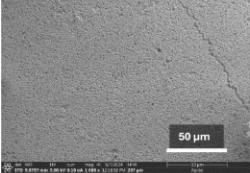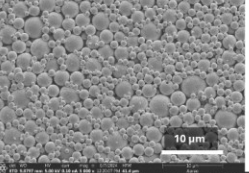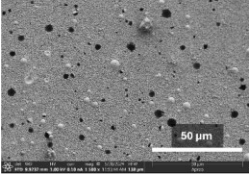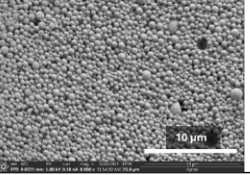
Lower Magnification Image	Higher Magnification Image	% PVA in 2nd w phase	Average Diameter (µm)	Maximum Diameter (µm)	Minimum Diameter (µm)	Polydispersity Index
		0.5	1.770	22.624	0.174	0.963
		1	1.242	3.772	0.280	0.671
		2	0.594	2.978	0.087	0.252

Figure 9: SEM images and data of dried double emulsion microspheres. SEM images have two scale bars of 50 and 10 µm. The concentration (wt%) of PVA in the second water phase is changed and the corresponding particle size information of each batch is given.

The results shown in Figure 9 indicate that the average diameter size of the solid double emulsion product particles is inversely related to the concentration of PVA in the second water phase of the double emulsion. The SEM images in Figure 9 confirm that the microspheres are distinct and suggest that the polydispersity index of the product is likewise inversely related to the concentration of PVA in the second water phase. It was observed that double emulsions prepared with 2 wt% PVA in the outer water phase produced the smallest and most uniform product particles.

5.3.5 Drying Methods

Several parameters relating to drying the double emulsions were examined, including the solvent evaporation method, vessel type, and drying time. The evaporation techniques include convection drying in a fume hood, convection drying in a fume hood with a stir bar, and freeze drying. The presence of a magnetic stir bar during solvent evaporation caused the

droplets to collect on the stir bar due to their superparamagnetic properties, disrupting the necessary double emulsion mechanism for spherical product particles. The final products, formed by convection drying and freeze drying, are compared in Figure 10.
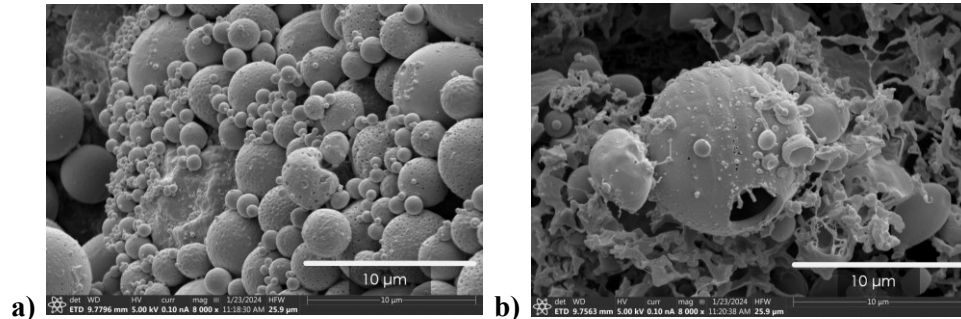
Figure 10: SEM images of double emulsion product particles with 1 wt% PVA in the outer water phase prepared with different drying methods **a)** convection drying, **b)** freeze drying. Scale bars are 10 μm.

Figure 10 demonstrates that freeze drying the double emulsions results in a significant presence of PLA debris in the final product which is not present when dried by convection. A reasonable hypothesis is that during cooling, but before freezing, there is a sol-gel microphase separation and then during freeze drying the polymer in the sol phase deposits on the surface of spherical particles.

An additional observation of freeze drying was the attraction of smaller product particles to the surface of larger product particles. Figure 11 demonstrates this interaction between freeze dried double emulsion material.
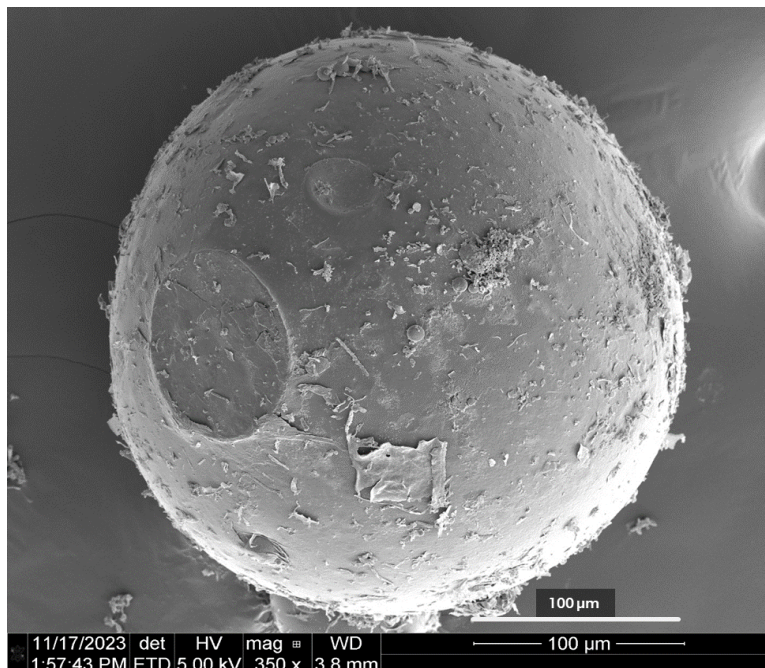
Figure 11: SEM image of a double emulsion product particle over 100 µm in diameter and a collection of debris and product microspheres under 10 µm in size on its surface. Product was synthesized with PVA in both water phases (9 wt% in inner water phase and 1 wt% in outer water phase) prepared by freeze drying.

The collection of debris and smaller microspheres on the surface of larger product microspheres as depicted in Figure 11 demonstrates the observed attraction of small, freeze-dried product to larger structures. It is likely that this attraction occurs before sublimation, causing smaller droplets and debris to dry after collection onto larger surfaces. This behavior is not desirable for product microspheres as it complicates both the dispersion of the product into a medium and the separation of target-size product from oversized product.

Although freeze drying did not produce microspheres of the desired size or behavior, it did produce microspheres with fractured surfaces allowing for easy observation and excellent image quality of the product interior. A fractured microsphere prepared by freeze drying is compared to the cross section of a convection dried microsphere in Figure 12.
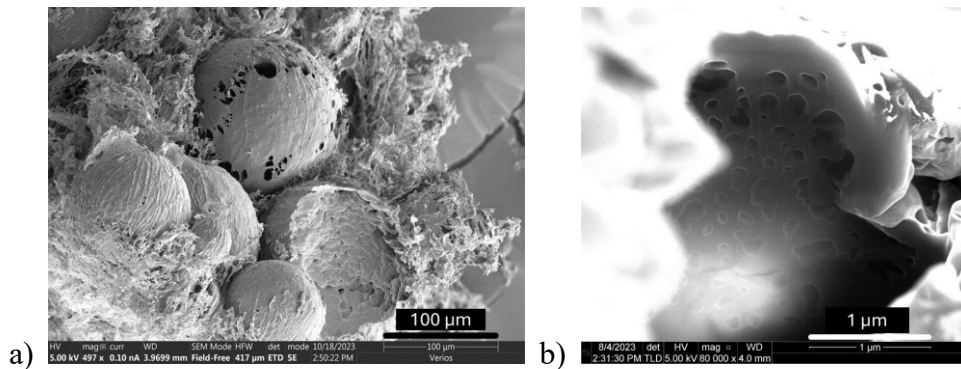
Figure 12: SEM image of a double emulsion microsphere with a significant fracture revealing its interior **a)** prepared by freeze drying, **b)** prepared by convection drying. Microspheres were made with PVA in both water phases (9 wt% in inner water phase and 1 wt% in outer water phase) prepared by freeze drying.

The microsphere depicted in Figure 12a contains a nexus of microchannels and structural shelfing formed by solvent evaporation during freeze drying. The particle cross section in Figure 12b reveals a network of spherical and nonspherical holes formed by solvent evaporation during convection drying, indicative of the submicron diameters of the inner water phase droplets. These interior structures confirm that drying by natural convection is more effective than freeze drying in achieving the desired internal structure consisting of non-connected spherical holes.

The vessels used for drying the product by convection in a fume hood were a petri dish and a watch glass. The double emulsion was about 5 mm deep in the petri dish and at the center of the watch glass. During the convective solvent removal process, there was sometimes a PLA film

observed to nucleate over the exposed surface of the double emulsion. Diluting the sample before convective drying was observed to reduce the thickness of the film. This film was also observed to form in response to disturbance of the vessel in which the sample was drying. The film was observed to form when the sample was stretched thin across the vessel's surface, suggesting that some nucleation process initiates film formation. If the film was physically extracted from the sample's surface, a new film was observed to form for as long as there was liquid suspension. Additionally, this film sometimes formed over the entire course of the drying phase if the vessel was left undisturbed and unwashed. This film could be physically peeled back to reveal the final, dried product underneath. For this drying process, a watch glass may be a more desirable vessel than one of more uniform level vessels like a petri dish. The film formed by samples dried in a watch glass were observed to be significantly thinner than samples dried in a petri dish. Figure 13 compares the product particles when dried in a petri dish and in a watch glass.
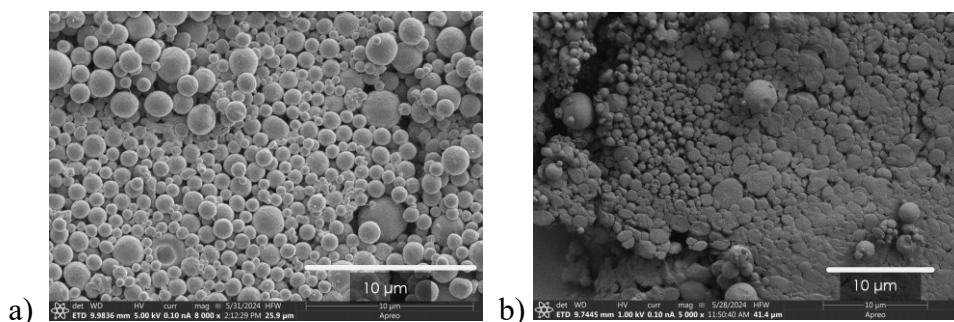
Figure 13: SEM images of double emulsion product particles with 1 wt% PVA in the outer water phase dried in **a)** a watch glass, **b)** a petri dish. Scale bars are 10 µm.

Microspheres produced by drying in a petri dish were frequently observed to be less distinctly spherical, but appeared slightly flattened, as illustrated in Figure 13. This figure also compares the typical particles produced after drying by watch glass and by petri dish, suggesting that drying the particles in a watch glass results in product significantly more spherical in nature.

The most crucial parameter tested was the drying time. It was found that redispersion of the double emulsion droplets in the water medium after completion of solvent evaporation was paramount to minimizing the diameter size of the product particles and to creating spherical uniformity. Lost solvent mass was replaced with distilled water before this redispersion. For a sample 3 mL in volume, the presence of $MeCl_2$ was no longer observable after 48 hours by olfaction, at which time the water was added. The particles produced by similar processes with and without this additional dispersion step are compared in Figure 14.

a)   b)
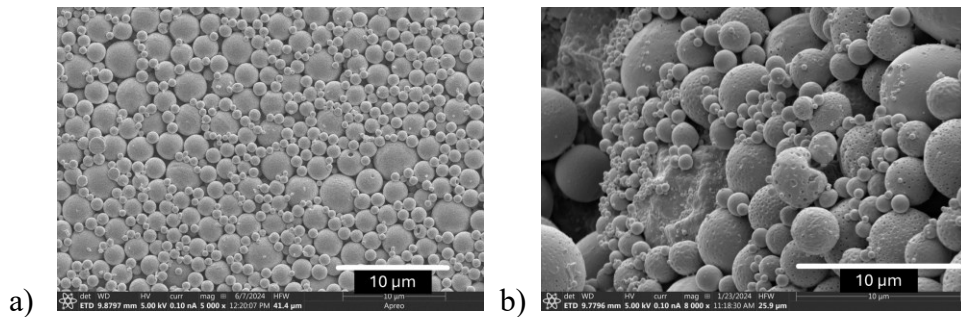
Figure 14: SEM images of double emulsion product particles with 1 wt% PVA in the outer water phase dried by convection **a)** replacing the mass of solvent lost by evaporation with distilled water and redispersing the emulsion before drying, **b)** without the additional wash, replacement, and redispersion step. Scale bars are 10 µm.

The results depicted by Figure 14 indicate that redispersion after solvent evaporation produces the particle diameter size within the desired target range. Because the small particles are the same size in both images, we speculate that without redispersion, some droplets coalesce to form the much larger particles in Figure 14b.

It was also frequently observed that the lack of a redispersion step caused the double emulsion droplets to agglomerate to one another before drying, as depicted in Figure 15.
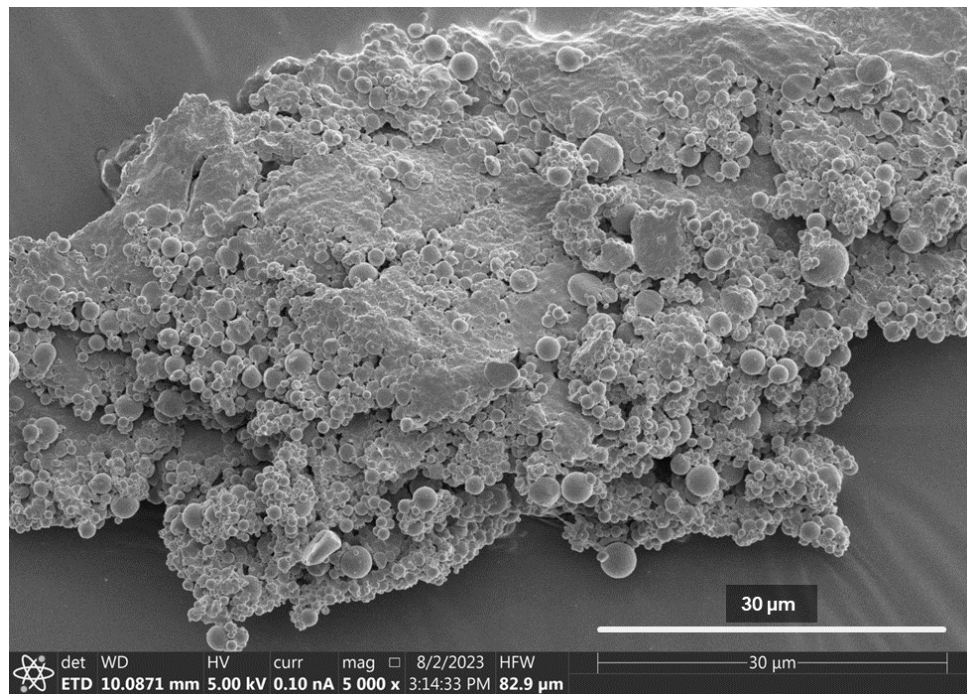
Figure 15: SEM image of double emulsion product particles with PVA in both water phases (9 wt% in inner water phase and 1 wt% in outer water phase) prepared by convection drying without the redispersion step.

Figure 15 shows a gradient of spherical morphology in product double emulsion microparticles. One may observe distinct spheres on the surface of the large agglomeration depicted in the figure, as well as product that gradually becomes less spherical and less distinct as the collection of product becomes a single agglomerated mass. This observation suggests that the presence of $MeCl_2$ in the sample during the drying step significantly alters the distinct spherical shape desired of the product microparticles. Therefore, the redispersion of the double emulsion in water after completion of solvent evaporation and before water evaporation is salient to producing consistently distinct product microspheres under 5 μm in diameter.

5.4   Resulting Optimal Procedure

In consideration of the results obtained from Section 5.3, the optimized and detailed procedure is described here.

5.4.1   Double Emulsion Phase Compositions

The first water phase was prepared by dissolving 60 mg of 5FU and 500 mg of polyvinyl alcohol (PVA) in 5 mL of distilled water. The organic phase was prepared by dissolving 3 g of PLA in 17 mL of $MeCl_2$. The SPION dispersion was created by dispersing 10 mg of SPIONs (9 nm in diameter) in 20 mL of $MeCl_2$ by sonication in a sonicating bath for 1 hour. Then 1 g of the SPION dispersion was added to 4 g of the PLA/$MeCl_2$, resulting in 0.088 mg of SPIONs per mg of organic phase and 0.094 mg of PLA per mg of organic phase. The resulting organic phase mixture was then vortexed for one minute.

The second (outer) water phase consisted of water and dissolved PVA at a concentration of 2 wt%.

5.4.2   Emulsion Mixing Methods

The first emulsion (w/o) was formed by adding 0.125 g of the first water phase to 4.875 g of the organic phase in a 20 mL scintillation vial. The resulting emulsion was then sonicated using a sonicating probe at an amplitude of 15% power (1.5 W/cm^2) for one minute in an ice bath, and then vortexed for one minute.

The second emulsion (w/o/w) was formed by adding 1 g of the first emulsion (w/o) to 4 g of the second water phase. The resulting emulsion was sonicated using the sonicating probe at the same amplitude of 15% for 3 minutes in an ice bath. The typical volume of double emulsion before sonication is 5 mL.

5.4.3   Emulsion Drying Method

5 mL of the double emulsion in a scintillation vial was placed in a 10 mm watch glass in a fume hood for 48 hours to evaporate the $MeCl_2$. Lost mass was replaced with distilled water. Then, the emulsion was redispersed using the sonicating probe at the same amplitude of 15% for one minute in an ice

bath. After redispersion, the w/o/w emulsion was dried at room temperature in a fume hood for 24 hours to dry.

Concentration of 5FU can be calculated from absorbance using Equation 6.1 where C is the concentration, A is the absorbance at 270 nm, ε is the molar extinction coefficient, and L is the optical path length.

$$C = \frac{A}{\varepsilon L} \tag{6.1}$$

The absorbance was obtained from a UV-VIS at a wavelength of 270 nm, a midpoint within a range of acceptable absorbance wavelengths for 5FU in current literature [61-63]. The optical path length is 1 cm, which is the interior width of the cuvette used for UV-VIS. The molar extinction coefficient was calculated by measuring the absorption of 5FU at various concentrations of 5FU dissolved in water. The data was plotted as absorption vs concentration of 5FU in Figure 16. The data was found to be linear through 1.24 absorbance units with the slope of the resulting trendline yielding the molar extinction coefficient of 830 cm^2/mg.
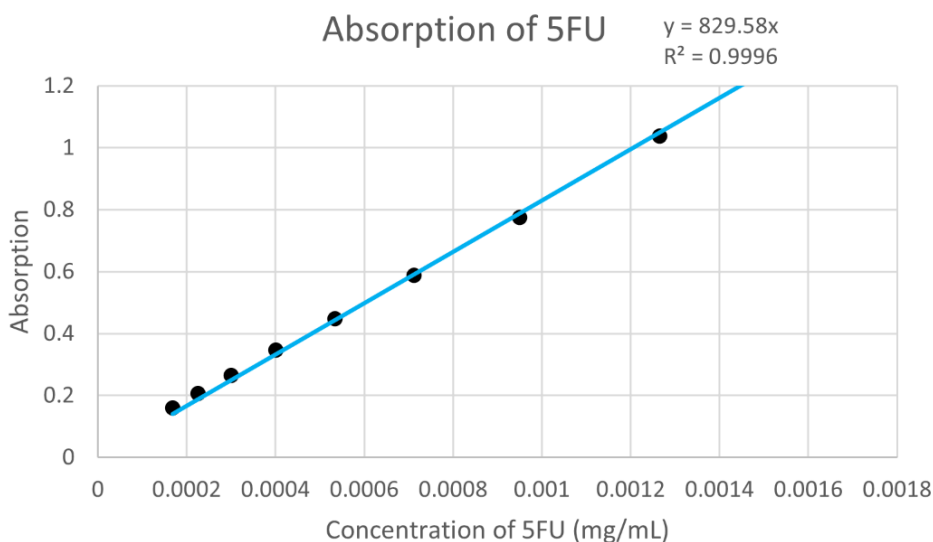
Figure 16: The absorption of 5FU at a wavelength of 270 nm as measured by UV-VIS is plotted vs the corresponding concentration of 5FU present in each measured sample (black). The line of best fit (blue) is represented in the form of the equation $y = mx + b$.

With this calculation, concentration of 5FU may be determined from absorbance measured using a UV-VIS and Equation 6.1.

The mass of 5FU encapsulated by the double emulsion microspheres was determined first by using Equation 6.1 to measure the absorbance of 5FU in a water medium after solvent evaporation and before redispersion in water. This sample was obtained by magnetically separating the emulsion droplets to the bottom so their 5FU was not measured. This measurement gave the mass of 5FU not encapsulated by the double emulsion system, so the difference between the total mass and this value then yielded the mass of 5FU encapsulated by the double emulsion system. Drug loading efficiency was then calculated using Equation 6.2,

$$Drug\ Loading\ Efficiency = \frac{Mass\ of\ Encapsulated\ 5FU}{Total\ Mass\ of\ 5FU}, \quad (6.2)$$

and was determined to be 99.6%. Comparable literature reports drug loading efficiencies around 95% for double emulsion PLA microspheres containing bacterial antigens or proteins and without SPIONs [52, 64]. A challenge in reporting drug loading efficiency with microspheres loaded with hydrophilic drug and composed of PLA is that polymer degradation begins as soon as the solid microspheres come in contact with the water or PBS medium. Magnetic separation of the suspended dry product for the purpose of UV-VIS spectrometry takes one hour, which is sufficient time for burst release to occur from the microspheres. Encapsulation efficiency was therefore determined by measuring the mass of 5FU decanted from the partially dried emulsion rather than from the suspended solid product to avoid interference from early burst release of the drug. The remarkably high drug loading efficiency calculated in this project could therefore be attributed to the nontraditional method of measurement necessitated by use of hydrophilic drug in tandem with biodegradable polymer.

7 *Drug Release Kinetics from Polymeric Microspheres*

7.1 Controlled Drug Release Measurements

Dried microspheres (25 mg) were added to 5 mL of the release medium in a 6 mL scintillation vial. The contents were then sonicated for 1 minute using the sonicating probe at an amplitude of 15% instrument power (~1.5 W/cm^2) to fully disperse the microspheres in the medium. Vials containing the microsphere dispersion were secured in a rotating frame (45 RPM) (see Figure 17) to maintain constant convection within the vials and prevent the microspheres from settling.

Figure 17: Drug release convection and temperature control setup. Vials are contained in a cylinder (black) placed on a rotating frame (blue) within an oven.

At each specified time point, a vial was removed from the rotating frame and placed on top of a strong magnet for 1 hour to magnetically separate the microspheres from the release medium. After separation, 3 mL of the

release medium were transferred to a 4 mL cuvette via pipette to measure absorbance with the UV-VIS Spectrometer. The absorbance was measured at a wavelength of 270 nm, a midpoint within a range of absorbance for 5FU [7, 8, 19]. The cuvette and its contents were discarded, and 3 mL of fresh release medium were added to the sample vial. The sample was then vortexed for 30 seconds and returned to the rotating frame until the next time interval.

Controlled drug release was evaluated using the procedure described above while varying four key parameters of the release experiment: 1) the concentration of PVA in the outer water phase of the double emulsion prepared during synthesis (0.5, 1, and 2 wt% of the outer water phase), 2) the polymer used in the organic phase of the double emulsion during synthesis (PLA and PLGA), 3) the release medium and its pH (PBS at pH 5.4 and 7.4 and distilled water at pH 7.0), and 4) the temperature of the release environment (37 °C and 21 °C). The standard procedure for drug release with no modified parameters was performed with a 1) 2 wt%, 2) PLA, 3) PBS with a pH of 7.4, and 4) 37 °C.

Three release experiments were performed for each formulation (composition) or condition (temperature, pH, etc.) Samples were taken at exact times so that a paired comparison could be done, with 3 sets of paired data for each formulation or condition. Statistical analysis was done using conventional paired comparison and Student-t statistics to calculate one-sided T-values and p-values. Statistical significance was attributed to data when $p < 0.05$. For clarity in the plots presented below, the datum point signifies the mean of the 3 measurements, and the whiskers denote the range of the measurements.

7.2   Drug Release Results and Kinetics

The standard release, which is the base-case against which other release will be compared, into PBS at a pH of 7.4 in an environment of 37 °C from a PLA microparticle made by a double emulsion technique which included 2 wt% of PVA in the outer water phase, is depicted in Figure 18.
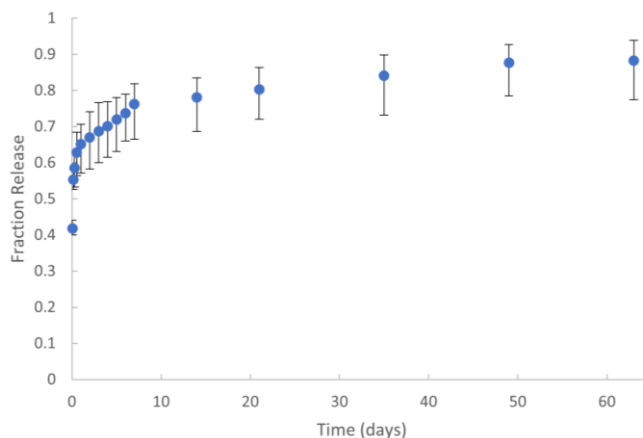
Figure 18: Fraction of 5FU released from standard microspheres with base-case parameters: 2 wt% PVA in the outer water phase, PLA as the organic phase polymer, PBS with pH 7.4 as the release medium, and the release environment temperature of 37 °C. The brackets show the range of data, and each datum point is the mean of the data.

The standard release data (see Figure 18) can be characterized as a faster release within the first day with a tight range, followed by a slower, constant release for 6 days, and then an even slower but constant release. Total release is not achieved during this time. Particles were still observed in the samples at 63 days. The kinetics of drug release from PLA structures in general is highly dependent on the characteristics of the particles and is most often described as having a slight sigmoidal shape due to polymer degradation [65-67]. This shape can be envisioned in Figure 18, but with the initial increasing rate of release replaced with a burst release normally observed in spherical PLA structures [68, 69]. The release kinetics of the particles can be described as follows: a burst release at 1 hr (the first point on Figure 18), a quick release through 1 day, a near constant release until 7 days, and a decrease in rate of release until completion.

For comparison, drug release of 5FU from microspheres with varying concentrations of PVA is described in Figure 19.
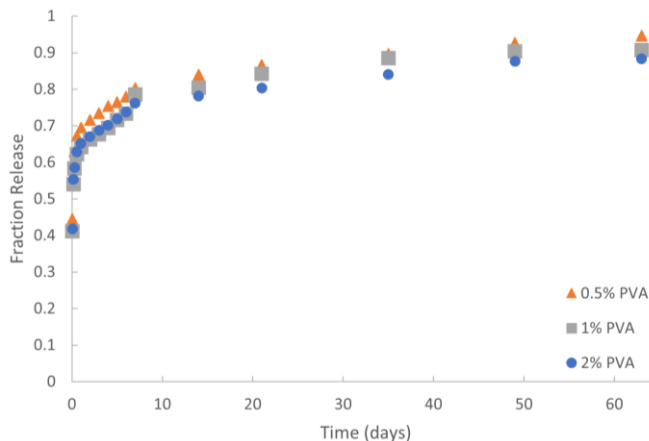
Figure 19: Fraction of 5FU released from microspheres with formulated 0.5, 1, and 2 wt% PVA in the outer water phase of the double emulsion. The organic phase polymer used during synthesis was PLA. The release medium was PBS with a pH of 7.4. The temperature of the release environment was 37 °C. For clarity, the range bars are not shown but are about the same size as in Figure 18.

The PVA concentrations of 0.5% and 1% were not statistically different ($p > 0.05$) from the standard experiment at all time points.

I have previously shown that the concentration of PVA in the outer water phase of the double emulsion microspheres is inversely related to the diameter of the resulting product microspheres (see Section 5.3.4). SEM analysis revealed that the samples prepared in this study with 0.5%, 1%, and 2% PVA had average diameters of 1.770, 1.242, and 0.594 μm respectively.

A decrease in size (average diameter) suggests an increase in total surface area of the spherical product. Furthermore, comparable literature shows that particle size of PLA/PLGA structures is inversely related to the speed of drug release [65, 66, 70]. Therefore, faster drug release in the samples prepared with a higher concentration of PVA was expected, but not observed. This observation may be attributed to unpredicted differences in the microspheres at the chemical level caused by varied concentrations of PVA.

Figure 20 reveals the difference in 5FU release between microspheres prepared using PLA versus PLGA as the organic phase polymer. Microspheres prepared using PLGA as the organic phase polymer were statistically different from the standard experiment only at times from 1 hr to 49 days.
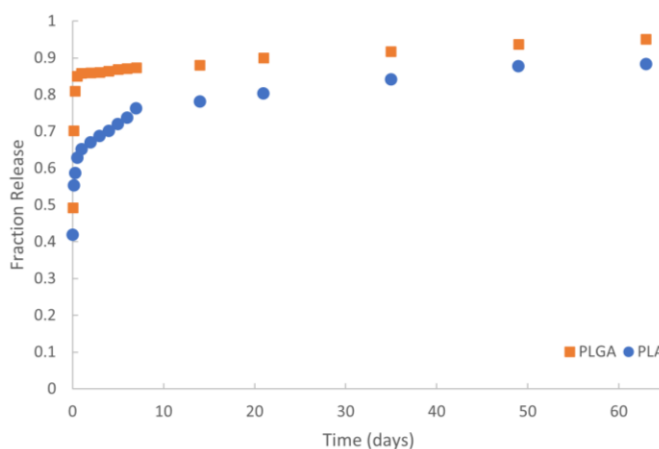
Figure 20: Fraction of 5FU released from microspheres with the organic phase polymer of PLA and PLGA. PVA concentration in the outer water phase of the double emulsion was 2%. The release medium was PBS with a pH of 7.4. The temperature of the release environment was 37 °C. For clarity, the range bars are not shown but are about the same size as in Figure 18.

The copolymer PLGA is usually less crystalline than PLA, leading to faster hydrolysis and subsequent polymer chain cleavage [67, 71]. Therefore, release behavior observed in Figure 20 is consistent with the expectation that PLA might degrade more slowly because it may be more crystalline than PLGA.

Figure 21 shows the effect of the release medium on 5FU release. The difference in 5FU release from these microspheres into various mediums appears to be insignificant over about 20 days, with the cumulative release into PBS of pH 5.4 appearing slightly less than into PBS of 7.4 and distilled water at pH 7.0 at 35 days. Additionally, Figure 21 shows the release into PBS of pH 5.4 in the first week as two near-linear segments (1-4 days and 4-7 days) and that of PBS of pH 7.4 and distilled water as a single near-linear segment across this interval. The release medium of PBS at pH 5.4 is statistically different from the standard experiment only at times from 1 hr

to 4 hrs. The release medium of water was not statistically different from the standard experiment at all time points.
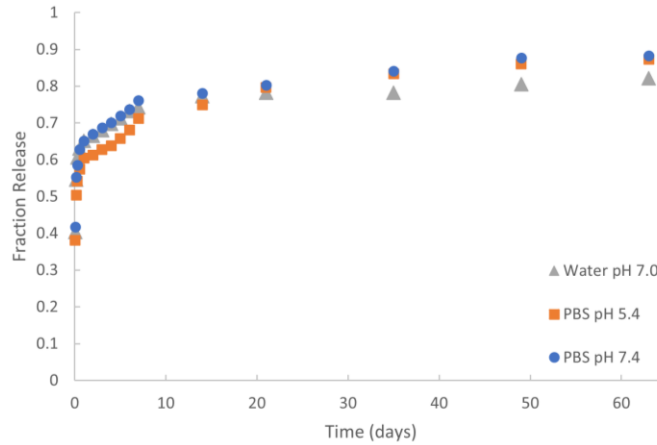
Figure 21: Fraction of 5FU released from microspheres into a release medium of distilled water at a pH of 7.0, PBS at a pH of 7.4, and PBS at a pH of 5.4. PVA concentration in the outer water phase of the double emulsion was 2%. The organic phase polymer used during synthesis was PLA. The release medium was PBS with a pH of 7.4. The temperature of the release environment was 37 °C. For clarity, the range bars are not shown but are about the same size as in Figure 18.

I chose pH levels of 7.4 and 5.4 to simulate the typical pH level in the human body and tumor environments respectively. Literature reports that a strongly acidic environment accelerates polymer degradation and that a slightly acidic pH environment (4-6 pH) decelerates polymer degradation compared to a neutral pH environment [71-74]. Therefore, a slightly slower 5FU release in the pH 5.4 medium was expected, which is consistent with the results shown in Figure 21 over the first 10 days of release.

The effect of the release environment temperature on 5FU release is compared in Figure 22. Figure 22 indicates that release at 21 °C is statistically different from the standard experiment at all time points. 5FU release in an environment of 37 °C is significantly higher than that of 21 °C for the entire duration of the release.
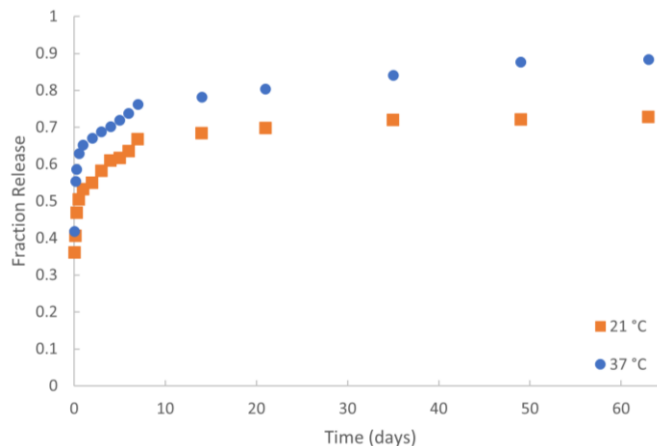
Figure 22: Fraction of 5FU released from microspheres with a release environment at the temperatures of 21 °C and 37 °C . PVA concentration in the outer water phase of the double emulsion was 2%. The organic phase polymer used during synthesis was PLA. The release medium was PBS with a pH of 7.4. For clarity, the range bars are not shown but are about the same size as in Figure 18.

The temperatures of 21 °C and 37 °C were chosen to simulate room temperature and the typical temperature of the human body. Polymer degradation of PLA increases as the temperature of the environment increases [74-76]. Thus, faster 5FU release was expected in the 37 °C environment than in the 21 °C environment, which is consistent with the findings reported in Figure 22.

8 *Antibiotic Potency and Chemical Integrity of 5FU After Release from Microspheres*

This section evaluates whether 5FU in the microspheres retains its effectiveness after incorporation. This was evaluated in a qualitative test of the potency against *S. aureus*, bacteria that is susceptible to 5FU, and in a comparison of 5FU absorbance spectra before and after release from the product microspheres.

8.1 Zone of Inhibition

A zone of inhibition test was performed to confirm the presence, release, and potency of 5FU in the microspheres using *S. Aureus* (see Figure 23). When *S. aureus* is spread, little colonies start to grow on the agar, seen as little white spots. Where the 5FU leaches from the piles of microspheres, the *S. aureus* is killed, so the white spots do not grow. When microspheres were placed on a bacteria colonized agar plate, bacterial growth was inhibited at a distance up to 10 mm from the microspheres, confirming the presence, release, and potency of 5FU in the microspheres.
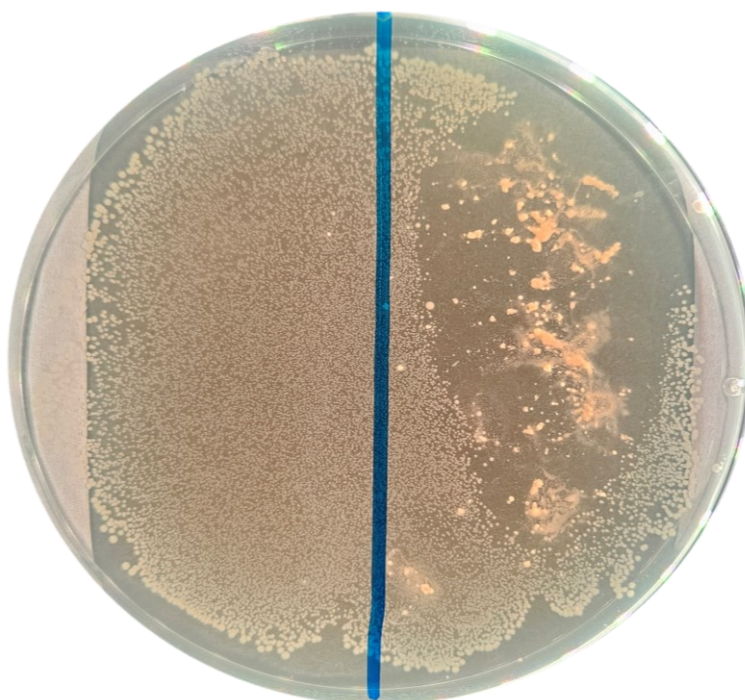
Figure 23: Picture of a zone of inhibition test performed using *S.* Aureus on a petri dish. The left half contains no 5FU and the right half contains the dried, synthesized microspheres.

8.2   Minimum Inhibitory Concentration

The minimum inhibitory concentration (MIC) of 5FU before and after release from the microspheres was also examined by the broth microdilution technique to confirm that the potency of the 5FU is maintained during release. This was done by growing *S. aureus* at 5 x 10^3 CFU/mL in nutrient broth with varying concentrations of 5FU. The smallest concentration of 5FU which inhibits the growth of the *S. aureus* is the MIC. Comparison of the absorbance spectra of 5FU before and after release showed no significant differences or new peaks. The similar 5FU absorbance spectra gathered indicate that the 5FU does not undergo any measurable chemical change during encapsulation and release.

8.3   5FU Absorbance Spectra Comparison

UV-VIS absorbance spectra were compared for 5FU before and after release from the product microspheres to confirm that no significant chemical change occurs in the 5FU during release. The MIC of 5FU before and after release was found to be 16 µg/mL. The identical MICs observed of 5FU before and after release suggest that the formulation and release process does not change the drug potency.

9 *Discussion*

9.1 Summary

This project produced PLA microspheres loaded with 5FU and SPIONs formed using a double emulsion method and carefully dried by solvent evaporation. Working with 5 mL of double emulsion suspension, about 25 mg of dried product was recovered after drying for 72 total hours These product particles had an average diameter as low as 0.594 μm with a polydispersity index of 0.252, were distinctly spherical in shape with a smooth surface, and exhibited superparamagnetic properties. With the goal of this project being to produce dried double emulsion PLA microspheres containing 5FU and SPIONs with the average and maximum particle diameter size below 5 μm distinctly spherical in shape, this goal was met.

The target size of 5 μm for microspheres in this project is optimal for application in cancer drug delivery to tumors because they are sufficiently small to be diverted into the surface of the endothelial cells lining the capillaries of a tumor by an external magnetic field where they can release their anticancer payload. The use of a Halbach array as an external magnetic field enables the microspheres to be magnetically pushed to a target point within the array rather than simply pulled toward a magnet itself [38]. Additional trials exploring the extent of particle size minimization using PVA could prove beneficial for specific drug release applications. Decreasing the particle diameter increases the overall surface area of the product, theoretically inducing a quicker rate of degradation and the drug release rate.

This project also evaluated the parameters for controlled release of 5FU from these PLA and PLGA microspheres loaded with 5FU and SPIONs. The standard microspheres with unmodified parameters (PVA concentration of 2 wt% in the outer water phase of the double emulsion, PLA as the organic phase polymer, PBS with a pH of 7.4 as the release medium, and a release environment temperature of 37 °C) release 5FU in the following segments: 1) a burst release at 1 hr, 2) an initially fast and decreasing release rate through day 1, 3) a near linear release until 7 days, 4) a decrease in rate of release until data collection was stopped on day 63. The effect of PVA concentration upon release rate in the outer water phase of the microparticle double emulsion prepared during synthesis appears to be insignificant or nonobvious for the concentrations of 0.5, 1, and 2 wt% of the outer water phase. The release of 5FU from these microspheres

composed of PLGA was significantly faster than those composed of PLA. The release of 5FU was slower in a slightly acidic environment of pH 5.4 than in a neutral environment of pH 7.4 over the first 10 days. 5FU release into PBS of pH 5.4 and 7.4 was faster than into distilled water of pH 7.0 after 20 days of release. 5FU release in a release environment temperature of 37 °C was significantly faster than that of 21 °C for the entire duration of the release.

The desired rate of release for a drug carrier depends on its application. This study provides drug release data in consideration of the scenario presented previously in which the microspheres are magnetically guided to the interior of a tumor [77]. Therefore, it presents drug release data necessary to induce a faster or slower release rate of 5FU from these microspheres depending on the configuration of the evaluated parameters.

9.2   Impact

This work appears to be the first report of spherical, solid PLA particles with a homogeneous distribution of SPIONs and hydrophilic anticancer drug with an average diameter less than 2 microns. Many studies have produced non-magnetic w/o/w double emulsion PLA or PLGA liquid microspheres loaded with drug with an average diameter above 10 μm [48, 78-84]. State of the art microspheres of a similar composition have been recorded with an average diameter under 10 μm and as low as 0.8 μm, but these were not magnetic [52, 64]. Double emulsion experiments using PLA as the polymer and 25-mer-FITC-labelled oligonucleotide as the payload have yielded particles as small as 0.45 μm in average diameter, but these particles were reportedly aspherical, aggregated, invaginated, and non-magnetic [50]. Some of the smallest polyester particles loaded with a payload for biomedical application were reported by a classic study which produced porous PLGA particles loaded with proteins at an average diameter below 0.1 μm. However, these particles are not solid spheres, are nonmagnetic, and were prepared by phase inversion rather than double emulsion.

Many studies have produced magnetic microspheres with an Fe_3O_4 core and a PLA shell rather than a PLA microsphere with Fe_3O_4 SPIONsand drug distributed throughout the structure. One such study produced microspheres over 50 μm in diameter with an Fe_3O_4 core and a PLA shell [85]. Experiments have produced microspheres with an Fe_3O_4 core and PLA shell under 2 μm in diameter using the complex method of electrohydrodynamic atomization [86]. A unique study produced nanospheres under 10 nm in diameter encapsulating the hydrophobic anticancer drug curcumin within the PLA-PEG shell which coats the Fe_3O_4 core for controlled release and hyperthermic cancer therapy [51]. The PLA microspheres with Fe_3O_4 and hydrophilic drug distributed within the structure presented in this study are unique and simple to produce.

Additionally, the drug release data presented may widen the application of these microspheres in future research and clinical trials.

9.3 Recommendations for Future Work

Future work should evaluate drug release as smaller increments within the first hour to determine the release rate of the burst release, which would require the application of a quicker separation method. Barrier films such as silicone could be explored to retard drug release from the surface and reduce burst release for applications where immediate release is not desired [87]. Enteric coatings like shellac or hydroxypropyl methyl cellulose (HPMC) could also be explored to delay release in the non-alkaline environments to which the microspheres would be expected to travel [88]. Release of doxorubicin could be explored, loaded in either the water or organic phase, as it is a widely researched anticancer drug and can be manipulated with pH to be more hydrophilic or hydrophobic. The small single emulsions from this study could be examined in future research, with drug in the inner phase. Combined therapy of drug delivery and hyperthermia could be explored using these microspheres and an alternating magnetic field targeting the SPIONs. The influence of an alternating magnetic field on the SPIONs may induce an increase in temperature, further increasing the degradation rate of the particles and release rate of the drug [51, 89-92].

10 *References*

[1]   C. Pucci, C. Martinelli, and G. Ciofani, "Innovative approaches for cancer treatment: current perspectives and new challenges," *Ecancermedicalscience,* vol. 13, Sep 10, 2019.

[2]   L. Wyld, R. A. Audisio, and G. J. Poston, "The evolution of cancer surgery and future perspectives," *Nature Reviews Clinical Oncology,* vol. 12, no. 2, pp. 115-124, Feb, 2015.

[3]   M. Bierbaum, F. Rapport, G. Arnolda, B. N. G. Easpaig, K. Lamprell, K. Hutchinson, G. P. Delaney, W. Liauw, R. Kefford, I. Olver, and J. Braithwaite, "Clinicians' attitudes and perceived barriers and facilitators to cancer treatment clinical practice guideline adherence: a systematic review of qualitative and quantitative literature," *Implementation Science,* vol. 15, no. 1, May 27, 2020.

[4]   R. Sullivan, O. I. Alatise, B. O. Anderson, R. Audisio, P. Autier, A. Aggarwal, C. Balch, M. F. Brennan, A. Dare, A. D'Cruz, A. M. M. Eggermont, K. Fleming, S. M. Gueye, L. Hagander, C. A. Herrera, H. Holmer, A. M. Ilbawi, A. Jarnheimer, J. F. Ji, T. P. Kingham, J. Liberman, A. J. M. Leather, J. G. Meara, S. Mukhopadhyay, S. S. Murthy, S. Omar, G. P. Parham, C. S. Pramesh, R. Riviello, D. Rodin, L. Santini, S. V. Shrikhande, M. Shrime, R. Thomas, A. T. Tsunoda, C. van de Velde, U. Veronesi, D. K. Vijaykumar, D. Watters, S. Wang, Y. L. Wu, M. Zeiton, and A. Purushotham, "Global cancer surgery: delivering safe, aff ordable, and timely cancer surgery," *Lancet Oncology,* vol. 16, no. 11, pp. 1193-1224, Sep, 2015.

[5]   J. H. Krouse, H. J. Krouse, and R. L. Fabian, "Adaptation to Surgery for Head and Neck-Cancer," *Laryngoscope,* vol. 99, no. 8, pp. 789-794, Aug, 1989.

[6]   Q. F. Li, Y. Tie, A. Alu, X. L. Ma, and H. S. Shi, "Targeted therapy for head and neck cancer: signaling pathways and clinical studies," *Signal Transduction and Targeted Therapy,* vol. 8, no. 1, Jan 16, 2023.

[7]   P. Sharma, V. Jhawat, and P. Mathur, "Innovation in cancer therapeutics and regulatory perspectives," *Medical Oncology,* vol. 39, no. 5, May, 2022.

[8]   C. Lindley, J. S. McCune, T. E. Thomason, D. Lauder, A. Sauls, S. Adkins, and W. T. Sawyer, "Perception of chemotherapy side effects - Cancer versus noncancer patients," *Cancer Practice,* vol. 7, no. 2, pp. 59-65, Mar-Apr, 1999.

[9]   A. Pearce, M. Haas, R. Viney, S. A. Pearson, P. Haywood, C. Brown, and R. Ward, "Incidence and severity of self-reported chemotherapy side effects in routine care: A prospective cohort study," *Plos One,* vol. 12, no. 10, Oct 10, 2017.

[10]   W. M. C. van den Boogaard, D. S. J. Komninos, and W. P. Vermeij, "Chemotherapy Side-Effects: Not All DNA Damage Is Equal," *Cancers,* vol. 14, no. 3, Feb, 2022.

[11]   M. Nagane, H. J. S. Huang, and W. K. Cavenee, "The potential of TRAIL for cancer chemotherapy," *Apoptosis,* vol. 6, no. 3, pp. 191-197, Jun, 2001.

[12]   M. Nieminen, K. Aro, A. Makitie, V. Harlin, S. Kainulainen, L. Jouhi, and T. Atula, "Challenges in diagnosing head and neck cancer in primary health care," *Annals of Medicine,* vol. 53, no. 1, pp. 26-33, Jan 1, 2021.

[13]   J. S. Tobias, "Current Issues in Cancer - Cancer of the Head and Neck," *British Medical Journal,* vol. 308, no. 6934, pp. 961-966, Apr 9, 1994.

[14]   A. Starzynska, B. K. Sobocki, and D. Alterio, "Current Challenges in Head and Neck Cancer Management," *Cancers,* vol. 14, no. 2, pp. 358, Jan, 2022.

[15]   G. R. Bhat, R. G. Hyole, and J. Li, "Head and neck cancer: Current challenges and future perspectives," *Advances in Cancer Research, Vol 152,* vol. 152, pp. 67-102, 2021.

[16]   E. Alsahafi, K. Begg, I. Amelio, N. Raulf, P. Lucarelli, T. Sauter, and M. Tavassoli, "Clinical update on head and neck cancer: molecular biology and ongoing challenges," *Cell Death & Disease,* vol. 10, pp. 540, Jul 15, 2019.

[17]   S. K. Kundu, and M. Nestor, "Targeted therapy in head and neck cancer," *Tumor Biology,* vol. 33, no. 3, pp. 707-721, Jun, 2012.

[18]   S. K. Sindhu, and J. E. Bauman, "Current Concepts in Chemotherapy for Head and Neck Cancer," *Oral and Maxillofacial Surgery Clinics of North America,* vol. 31, no. 1, pp. 145-+, Feb, 2019.

[19]   J. S. Cooper, T. F. Pajak, A. A. Forastiere, J. Jacobs, B. H. Campbell, S. B. Saxman, J. A. Kish, H. E. Kim, A. J. Cmelak, M. Rotman, M. Machtay, J. F. Ensley, K. S. C. Chao, C. J. Schultz, N. Lee, K. K. Fu, and R. T. O. G. 9501, "Postoperative concurrent radiotherapy and chemotherapy for high-risk squamous-cell carcinoma of the head and neck," *New England Journal of Medicine,* vol. 350, no. 19, pp. 1937-1944, May 6, 2004.

[20]   K. Nakano, "Progress of molecular targeted therapy for head and neck cancer in clinical aspects," *Molecular Biomedicine,* vol. 2, no. 1, May 30, 2021.

[21]   F. Oppel, M. Gorner, and H. Sudhoff, "The Potential of Tumor Debulking to Support Molecular Targeted Therapies," *Frontiers in Oncology,* vol. 10, Jun 18, 2020.

[22]   M. Goerner, T. Y. Seiwert, and H. Sudhoff, "Molecular targeted therapies in head and neck cancer - An update of recent developements -," *Head & Neck Oncology,* vol. 2, Apr 14, 2010.

[23]   K. Dorsey, and M. Agulnik, "Promising New Molecular Targeted Therapies in Head and Neck Cancer," *Drugs,* vol. 73, no. 4, pp. 315-325, 2013.

[24]   A. Luengo, D. Y. Gui, and M. G. Vander Heiden, "Targeting Metabolism for Cancer Therapy," *Cell Chemical Biology,* vol. 24, no. 9, pp. 1161-1180, Sep 21, 2017.

[25]   S. B. Kaye, "New antimetabolites in cancer chemotherapy and their clinical impact," *British Journal of Cancer,* vol. 78, pp. 1-7, 1998.

[26]   N. Zhang, Y. Yin, S. J. Xu, and W. S. Chen, "5-fluorouracil: Mechanisms of resistance and reversal strategies," *Molecules,* vol. 13, no. 8, pp. 1551-1569, Aug, 2008.

[27]   D. B. Longley, T. Latif, J. Boyer, W. L. Allen, P. J. Maxwell, and P. G. Johnston, "The interaction of thymidylate synthase expression with p53-regulated signaling pathways in tumor cells," *Seminars in Oncology,* vol. 30, no. 3, pp. 3-9, Jun, 2003.

[28]   W. B. Parker, and Y. C. Cheng, "Metabolism and Mechanism of Action of 5-Fluorouracil," *Pharmacology & Therapeutics,* vol. 48, no. 3, pp. 381-395, 1990.

[29]   S. Missailidis, *Anticancer Therapeutics,* p.^pp. 97: Wiley-Blackwell, 2008.

[30]   G. B. Morrison, A. Bastian, T. Dela Rosa, R. B. Diasio, and C. H. Takimoto, "Dihydropyrimidine dehydrogenase deficiency: a pharmacogenetic defect causing severe adverse reactions to 5-fluorouracil-based chemotherapy," *Oncol Nurs Forum,* vol. 24, no. 1, pp. 83-8, Jan-Feb, 1997.

[31]   M. C. Etienne, G. Milano, N. Renee, J. L. Lagrange, O. Dassonville, A. Thyss, M. Schneider, E. Francois, R. Fleming, and F. Demard, "[Population study of dihydropyrimidine dehydrogenase in cancer patients]," *Bull Cancer,* vol. 82, no. 9, pp. 705-10, Sep, 1995.

[32]   E. Borras, E. Dotor, A. Arcusa, M. J. Gamundi, I. Hernan, M. de Sousa Dias, B. Mane, J. A. Agundez, M. Blanca, and M. Carballo, "High-resolution melting analysis of the common c.1905+1G>A mutation causing dihydropyrimidine dehydrogenase deficiency and lethal 5-fluorouracil toxicity," *Front Genet,* vol. 3, pp. 312, 2012.

[33] C. P. Bean, and J. D. Livingston, "Superparamagnetism," *Journal of Applied Physics,* vol. 30, no. 4, pp. S120-S129, 2009.

[34] F. Alexis, E. M. Pridgen, R. Langer, and O. C. Farokhzad, "Nanoparticle Technologies for Cancer Therapy," *Drug Delivery*, M. Schäfer-Korting, ed., pp. 55-86, Berlin, Heidelberg: Springer Berlin Heidelberg, 2010.

[35] S. Palanisamy, and Y. M. Wang, "Superparamagnetic iron oxide nanoparticulate system: synthesis, targeting, drug delivery and therapy in cancer," *Dalton Trans,* vol. 48, no. 26, pp. 9490-9515, Jul 2, 2019.

[36] M. W. Freeman, A. Arrott, and J. H. L. Watson, "Magnetism in Medicine," *Journal of Applied Physics,* vol. 31, no. 5, pp. S404-S405, 2009.

[37] J. Estelrich, E. Escribano, J. Queralt, and M. A. Busquets, "Iron Oxide Nanoparticles for Magnetically-Guided and Magnetically-Responsive Drug Delivery," *International Journal of Molecular Sciences,* vol. 16, no. 4, pp. 8070-8101, Apr, 2015.

[38] A. Sarwar, A. Nemirovski, and B. Shapiro, "Optimal Halbach Permanent Magnet Designs for Maximally Pulling and Pushing Nanoparticles," *J Magn Magn Mater,* vol. 324, no. 5, pp. 742-754, Mar 1, 2012.

[39] A. S. Lubbe, C. Bergemann, H. Riess, F. Schriever, P. Reichardt, K. Possinger, M. Matthias, B. Dorken, F. Herrmann, R. Gurtler, P. Hohenberger, N. Haas, R. Sohr, B. Sander, A. J. Lemke, D. Ohlendorf, W. Huhnt, and D. Huhn, "Clinical experiences with magnetic drug targeting: a phase I study with 4'-epidoxorubicin in 14 patients with advanced solid tumors," *Cancer Res,* vol. 56, no. 20, pp. 4686-93, Oct 15, 1996.

[40] A. Nacev, C. Beni, O. Bruno, and B. Shapiro, "Magnetic nanoparticle transport within flowing blood and into surrounding tissue," *Nanomedicine (Lond),* vol. 5, no. 9, pp. 1459-66, Nov, 2010.

[41] A. Nacev, C. Beni, O. Bruno, and B. Shapiro, "The Behaviors of Ferro-Magnetic Nano-Particles In and Around Blood Vessels under Applied Magnetic Fields," *J Magn Magn Mater,* vol. 323, no. 6, pp. 651-668, Mar 1, 2011.

[42] M. Ledda, D. Fioretti, M. G. Lolli, M. Papi, C. Di Gioia, R. Carletti, G. Ciasca, S. Foglia, V. Palmieri, R. Marchese, S. Grimaldi, M. Rinaldi, and A. Lisi, "Biocompatibility assessment of sub-5 nm silica-coated superparamagnetic iron oxide nanoparticles in human stem cells and in mice for potential application in nanomedicine," *Nanoscale,* vol. 12, no. 3, pp. 1759-1778, Jan 21, 2020.

[43] H. Wei, Y. N. Hu, J. G. Wang, X. Gao, X. Y. Qian, and M. L. Tang, "Superparamagnetic Iron Oxide Nanoparticles: Cytotoxicity,

Metabolism, and Cellular Behavior in Biomedicine Applications," *International Journal of Nanomedicine,* vol. 16, pp. 6097-6113, 2021.

[44] M. E. Ozgur, A. Ulu, S. Balcioglu, I. Ozcan, S. Koytepe, and B. Ates, "The Toxicity Assessment of Iron Oxide (Fe(3)O(4)) Nanoparticles on Physical and Biochemical Quality of Rainbow Trout Spermatozoon," *Toxics,* vol. 6, no. 4, pp. 62, Oct 18, 2018.

[45] T. Ma, L. Wang, TingyuanYang, D. Wang, G. Ma, and S. Wang, "PLGA-lipid liposphere as a promising platform for oral delivery of proteins," *Colloids Surf B Biointerfaces,* vol. 117, pp. 512-9, May 1, 2014.

[46] S. K. Hema, A. Karmakar, R. K. Das, and P. Srivastava, "Simple formulation and characterization of double emulsion variant designed to carry three bioactive agents," *Heliyon,* vol. 8, no. 9, pp. e10397, Sep, 2022.

[47] A. Mashhadian, H. Afjoul, and A. Shamloo, "An integrative method to increase the reliability of conventional double emulsion method," *Analytica Chimica Acta,* vol. 1197, pp. 339523, Mar 8, 2022.

[48] N. Debotton, S. Garsiani, Y. Cohen, and A. Dahan, "Enabling oral delivery of antiviral drugs: Double emulsion carriers to improve the intestinal absorption of zanamivir," *International Journal of Pharmaceutics,* vol. 629, pp. 122392, Dec 15, 2022.

[49] S. O. Dozie-Nwachukwu, Y. Danyuo, J. D. Obayemi, O. S. Odusanya, K. Malatesta, and W. O. Soboyejo, "Extraction and encapsulation of prodigiosin in chitosan rnicrospheres for targeted drug delivery," *Materials Science & Engineering C-Materials for Biological Applications,* vol. 71, pp. 268-278, Feb 1, 2017.

[50] F. Delie, M. Berton, E. Allemann, and R. Gurny, "Comparison of two methods of encapsulation of an oligonucleotide into poly(D,L-lactic acid) particles," *International Journal of Pharmaceutics,* vol. 214, no. 1-2, pp. 25-30, Feb 19, 2001.

[51] P. Q. Thong, L. T. Huong, N. D. Tu, H. T. M. Nhung, L. Khanh, D. Manh, P. H. Nam, N. X. Phuc, J. Alonso, J. Qiao, S. Sridhar, H. Thu, M. H. Phan, and N. T. K. Thanh, "Multifunctional nanocarriers of Fe_3O_4@PLA-PEG/curcumin for MRI, magnetic hyperthermia and drug delivery," *Nanomedicine,* vol. 17, no. 22, pp. 1677-1693, Sep, 2022.

[52] N. Kofler, C. Ruedl, J. Klima, H. Recheis, G. Bock, G. Wick, and H. Wolf, "Preparation and characterization of poly-(D,L-lactide-co-glycolide) and poly-(L-lactic acid) microspheres with entrapped pneumotropic bacterial antigens," *Journal of Immunological Methods,* vol. 192, no. 1-2, pp. 25-35, Jun 10, 1996.

[53] C. Ye, and H. Chi, "A review of recent progress in drug and protein encapsulation: Approaches, applications and challenges," *Materials*

Science & Engineering C-Materials for Biological Applications, vol. 83, pp. 233-246, Feb 1, 2018.

[54]   T. T. T. Trang, M. Mariatti, H. Badrul, K. Masakazu, X. T. T. Nguyen, and A. A. H. Zuratul, "Drug Release Profile Study of Gentamicin Encapsulated Poly(lactic Acid) Microspheres for Drug Delivery," *Materials Today: Proceedings*, pp. 836-845, 2019.

[55]   D. M. Rata, A. N. Cadinoiu, L. I. Atanase, G. Calin, and M. Popa, "Design and characterization of dexamethasone phosphate -loaded microcapsules obtained by a double-emulsion method," *International Journal of Pharmaceutics,* vol. 639, pp. 122971, May 25, 2023.

[56]   S. H. Sun, H. Zeng, D. B. Robinson, S. Raoux, P. M. Rice, S. X. Wang, and G. X. Li, "Monodisperse MFe2O4 (M = Fe, Co, Mn) nanoparticles," *Journal of the American Chemical Society,* vol. 126, no. 1, pp. 273-279, Jan 14, 2004.

[57]   K. Chesnel, M. Trevino, Y. Cai, J. Hancock, S. Smith, and R. Harrison, "Particle size effects on the magnetic behaviour of 5 to 11 nm Fe_3O_4 nanoparticles coated with oleic acid," *Journal of Physics: Conference Series,* vol. 521, pp. 012004, 06/06, 2014.

[58]   S. Klomp, C. Walker, M. Christiansen, B. Newbold, D. Griner, Y. Cai, P. Minson, J. Farrer, S. Smith, B. Campbell, R. Harrison, and K. Chesnel, "Size-dependent crystalline and magnetic properties of 5 to 100 nm Fe_3O_4 nanoparticles: superparamagnetism, Verwey transition and FeO-Fe_3O_4 core-shell formation," *IEEE Transactions on Magnetics,* vol. PP, pp. 1-1, 08/20, 2020.

[59]   K. Freeman, M. Connock, E. Cummins, T. Gurung, S. Taylor-Phillips, R. Court, M. Saunders, A. Clarke, and P. Sutcliffe, "Fluorouracil plasma monitoring: systematic review and economic evaluation of the My5-FU assay for guiding dose adjustment in patients receiving fluorouracil chemotherapy by continuous infusion," *Health Technology Assessment,* vol. 19, no. 91, pp. I-321, Nov, 2015.

[60]   J. F. Zheng, and H. D. Wang, "5-Fluorouracil concentration in blood, liver and tumor tissues and apoptosis of tumor cells after preoperative oral 5'-deoxy-5-fluorouridine in patients with hepatocellular carcinoma," *World Journal of Gastroenterology,* vol. 11, no. 25, pp. 3944-3947, Jul 7, 2005.

[61]   M. Szota, K. Reczynska-Kolman, E. Pamula, O. Michel, J. Kulbacka, and B. Jachimska, "Poly(amidoamine) Dendrimers as Nanocarriers for 5-Fluorouracil: Effectiveness of Complex Formation and Cytotoxicity Studies," *International Journal of Molecular Sciences,* vol. 22, no. 20, Oct, 2021.

[62] R. Ortiz, J. Prados, C. Melguizo, J. L. Arias, M. A. Ruiz, P. J. Alvarez, O. Caba, R. Luque, A. Segura, and A. Aránega, "5-Fluorouracil-loaded poly(ε-caprolactone) nanoparticles combined with phage gene therapy as a new strategy against colon cancer," *International Journal of Nanomedicine,* vol. 7, pp. 95-107, 2012.

[63] M. L. Pascu, M. Brezeanu, L. Voicu, A. Staicu, B. Carstocea, and R. A. Pascu, "5-Fluorouracil as a phosensitiser," *In Vivo,* vol. 19, no. 1, pp. 215-220, Jan-Feb, 2005.

[64] O. J. Mezu-Ndubuisi, Y. Y. Wang, J. Schoephoerster, and S. Q. Gong, "Intravitreal delivery of VEGF-A165-loaded PLGA microparticles reduces retinal vaso-obliteration in an mouse model of Retinopathy of Prematurity," *Investigative Ophthalmology & Visual Science,* vol. 59, no. 9, Jul, 2018.

[65] N. S. Berchane, K. H. Carson, A. C. Rice-Ficht, and M. J. Andrews, "Effect of mean diameter and polydispersity of PLG microspheres on drug release: Experiment and theory," *International Journal of Pharmaceutics,* vol. 337, no. 1-2, pp. 118-126, Jun 7, 2007.

[66] G. Acharya, C. S. Shin, K. Vedantham, M. McDermott, T. Rish, K. Hansen, Y. R. Fu, and K. Park, "A study of drug release from homogeneous PLGA microstructures," *Journal of Controlled Release,* vol. 146, no. 2, pp. 201-206, Sep 1, 2010.

[67] K. Avgoustakis, "Polylactic-co-glycolic acid (PLGA)," *Encyclopedia of biomaterials and biomedical engineering,* vol. 1, no. 1, pp. 1-11, 2005.

[68] S. Sant, M. Thommes, and P. Hildgen, "Microporous structure and drug release kinetics of polymeric nanoparticles," *Langmuir,* vol. 24, no. 1, pp. 280-287, Jan 1, 2008.

[69] T. Ehtezazi, and C. Washington, "Controlled release of macromolecules from PLA microspheres: using porous structure topology," *Journal of Controlled Release,* vol. 68, no. 3, pp. 361-372, Sep 3, 2000.

[70] F. J. Li, A. P. Zhu, X. L. Song, and L. J. Ji, "Novel surfactant for preparation of poly(L-lactic acid) nanoparticles with controllable release profile and cytocompatibility for drug delivery," *Colloids and Surfaces B-Biointerfaces,* vol. 115, pp. 377-383, Mar 1, 2014.

[71] H. K. Makadia, and S. J. Siegel, "Poly Lactic-co-Glycolic Acid (PLGA) as Biodegradable Controlled Drug Delivery Carrier," *Polymers,* vol. 3, no. 3, pp. 1377-1397, Sep, 2011.

[72] R. Vaid, E. Yildirim, M. A. Pasquinelli, and M. W. King, "Hydrolytic Degradation of Polylactic Acid Fibers as a Function of pH and Exposure Time," *Molecules,* vol. 26, no. 24, Dec, 2021.

[73] M. A. Elsawy, K. H. Kim, J. W. Park, and A. Deep, "Hydrolytic degradation of polylactic acid (PLA) and its composites," *Renewable & Sustainable Energy Reviews,* vol. 79, pp. 1346-1352, Nov, 2017.

[74] L. B. Xu, K. Crawford, and C. B. Gorman, "Effects of Temperature and pH on the Degradation of Poly(lactic acid) Brushes," *Macromolecules,* vol. 44, no. 12, pp. 4777-4782, Jun 28, 2011.

[75] K. L. G. Ho, A. L. Pometto, and P. N. Hinz, "Effects of temperature and relative humidity on polylactic acid plastic degradation," *Journal of Environmental Polymer Degradation,* vol. 7, no. 2, pp. 83-92, Apr, 1999.

[76] M. K. Mitchell, and D. E. Hirt, "Degradation of PLA fibers at elevated temperature and humidity," *Polymer Engineering and Science,* vol. 55, no. 7, pp. 1652-1660, Jul, 2015.

[77] Green TP, Harrison RG, Gautam R, Chesnel K, Pitt WG., "Synthesis of Biodegradable PLA Double Emulsion Microspheres for Magnetically Guided Drug Delivery of 5FU " *Journal of Drug Delivery Science and Technology,* vol. In Review, 2024.

[78] A. J. DeFail, H. D. Edington, S. Matthews, W. C. C. Lee, and K. G. Marra, "Controlled release of bioactive doxorubicin from microspheres embedded within gelatin scaffolds," *Journal of Biomedical Materials Research Part A,* vol. 79a, no. 4, pp. 954-962, Dec 15, 2006.

[79] D. H. R. Kempen, L. C. Lu, X. Zhu, C. Kim, E. Jabbari, W. J. A. Dhert, B. L. Currier, and M. J. Yaszemski, "Development of biodegradable poly(propylene fumarate)/poly(lactic-glycolic acid) blend microspheres.: II.: Controlled drug release and microsphere degradation," *Journal of Biomedical Materials Research Part A,* vol. 70a, no. 2, pp. 293-302, Aug 1, 2004.

[80] S. M. Lim, H. N. Eom, H. H. Jiang, M. Sohn, and K. C. Lee, "Evaluation of PEGylated Exendin-4 Released from Poly (Lactic-co-Glycolic Acid) Microspheres for Antidiabetic Therapy," *Journal of Pharmaceutical Sciences,* vol. 104, no. 1, pp. 72-80, Jan, 2015.

[81] H. J. Chung, I. K. Kim, T. G. Kim, and T. G. Park, "Highly open porous biodegradable microcarriers:: cultivation of chondrocytes for injectable delivery," *Tissue Engineering Part A,* vol. 14, no. 5, pp. 607-615, May, 2008.

[82] Y. Yang, N. Bajaj, P. Xu, K. Ohn, M. D. Tsifansky, and Y. Yeo, "Development of highly porous large PLGA microparticles for pulmonary drug delivery," *Biomaterials,* vol. 30, no. 10, pp. 1947-1953, Apr, 2009.

[83] R. S. Patel, D. Y. Cho, C. Tian, A. Chang, K. M. Estrellas, D. Lavin, S. Furtado, and E. Mathiowitz, "Doxycycline delivery from PLGA microspheres prepared by a modified solvent removal method," *Journal of Microencapsulation,* vol. 29, no. 4, pp. 344-352, 2012.

[84] A. Z. Faranesh, M. T. Nastley, C. P. de la Cruz, M. F. Haller, P. Laquerriere, K. W. Leong, and E. R. McVeigh, "In vitro release of

vascular endothelial growth factor from gadolinium-doped biodegradable microspheres," *Magnetic Resonance in Medicine,* vol. 51, no. 6, pp. 1265-1271, Jun, 2004.

[85] C. P. He, W. X. Zeng, Y. Su, R. W. Sun, Y. Xiao, B. L. Zhang, W. F. Liu, R. R. Wang, X. Zhang, and C. P. Chen, "Microfluidic-based fabrication and characterization of drug-loaded PLGA magnetic microspheres with tunable shell thickness," *Drug Delivery,* vol. 28, no. 1, pp. 692-699, Jan 1, 2021.

[86] S. Gun, M. Edirisinghe, and E. Stride, "Encapsulation of superparamagnetic iron oxide nanoparticles in poly-(lactide-co-glycolic acid) microspheres for biomedical applications," *Materials Science & Engineering C-Materials for Biological Applications,* vol. 33, no. 6, pp. 3129-3137, Aug 1, 2013.

[87] S. H. Choi, I. H. Cho, and S. Park, "Gemcitabine-incorporated polyurethane films for controlled release of an anticancer drug," *Biomaterials Research,* vol. 23, no. 1, 2019.

[88] H. El Mabrouki, and I. E. Kaukhova, "Formulation and Development of Aqueous Film Coating for Moisture Protection of Hygroscopic L. Tablets," *Turkish Journal of Pharmaceutical Sciences,* vol. 19, no. 2, pp. 153-160, Apr, 2022.

[89] M. Khaledian, M. S. Nourbakhsh, R. Saber, H. Hashemzadeh, and M. H. Darvishi, "Preparation and Evaluation of Doxorubicin-Loaded PLA-PEG-FA Copolymer Containing Superparamagnetic Iron Oxide Nanoparticles (SPIONs) for Cancer Treatment: Combination Therapy with Hyperthermia and Chemotherapy," *Int J Nanomedicine,* vol. 15, pp. 6167-6182, 2020.

[90] C. Caizer, and I. S. Caizer, "Study on Maximum Specific Loss Power in Fe3O4 Nanoparticles Decorated with Biocompatible Gamma-Cyclodextrins for Cancer Therapy with Superparamagnetic Hyperthermia," *International Journal of Molecular Sciences,* vol. 22, no. 18, Sep, 2021.

[91] R. Hergt, S. Dutz, R. Muller, and M. Zeisberger, "Magnetic particle hyperthermia: nanoparticle magnetism and materials development for cancer therapy," *Journal of Physics-Condensed Matter,* vol. 18, no. 38, pp. S2919-S2934, Sep 27, 2006.

[92] N. D. Thorat, R. A. Bohara, M. R. Noor, D. Dhamecha, T. Soulimane, and S. A. M. Tofail, "Effective Cancer Theranostics with Polymer Encapsulated Superparamagnetic Nanoparticles: Combined Effects of Magnetic Hyperthermia and Controlled Drug Release," *ACS Biomater Sci Eng,* vol. 3, no. 7, pp. 1332-1340, Jul 10, 2017.